Transient Liquid Phase Joining of Carbon and Stainless Steels to Aluminum Alloy Using Gallium Metal

BY

Yuke Wang
B.S. Chongqing University of Technology, Chongqing, China 2011

THESIS
Submitted as partial fulfillment of the requirements
for the degree of Master of Science in Materials Engineering
in the Graduate College of the
University of Illinois at Chicago, 2015
Chicago, Illinois

Defense Committee:

        Dr. J. Ernesto Indacochea – Chair and Advisor
        Dr. Michael J. McNallan, Civil and Materials Engineering
        Dr. Didem Ozevin, Civil and Materials Engineering

This thesis is dedicated to my mother, without her perpetual love and encouragement, it would never been accomplished.

ACKNOWLEDGMENTS

I would like to express my sincere appreciation to my advisor, Dr. J. Ernesto Indacochea, for his patient guidance, enthusiastic encouragement and valuable critiques of this work. Without his support, the thesis could not have been completed.

I would also like to thank my committee members, Dr. Michael J. McNallan and Dr. Didem Ozevin, for their support and evaluation of my work.

I wish to thank my colleagues at UIC, Sai Vadlamani, Eric Lee, Vineeth Kumar, Zheng Zhang and Pedro Bauer, for their help throughout this project.

Finally, I want to thank my families and my friends for their love and encouragement throughout my study.

TABLE OF CONTENTS

TABLE OF CONTENTS

CHAPTER	**PAGE**

LIST OF TABLES

LIST OF FIGURES

SUMMARY

An investigation on joining 1020 steel and 304L stainless steels to 6061 T-6 aluminum (Al) alloy was carried out by transient liquid phase (TLP) bonding using gallium (Ga) as the interlayer metal. The deposited gallium film was used as the active metal to produce a narrow transient liquid film to enhance bonding between the two substrates. Joints were fabricated using different bonding temperatures and holding times. The microstructures for each sample were examined via optical microscopy and scanning electron microscopy (SEM). Tensile tests were performed for representative samples from each bonding system. Micro-hardness profile across the bonding region for each sample was also obtained.

Sound bonds were obtained with the 1020 steel/Ga/6061 Al joint. The Fe_2Al_5 intermetallic compound was identified in the midst of reaction layers from SEM/EDS analysis and by the extreme hardness values obtained from micro-hardness measurements. The sample processed at 450ºC for 4 hours showed the highest tensile strength.

Strong bonds were also obtained for the 304L Stainless Steel/Ga/6061-Al joints. The bonding region was wider with an uneven reaction layer at the 6061-Al side and a much narrower reaction layer at the 304L SS side. The highest tensile strength was measured for the sample fabricated at 330ºC for 6 hours.

It was determined that the Ga-film promotes the formation of the narrow transient liquid layer that aided in the isothermal local solidification, and enhanced the inter-diffusion of the Fe

SUMMARY (continued)

and Al atoms. In addition, Ga diffuses quicker and to a greater extent in the 6061-Al base metal. It

was also observed that the excess Ga and the overaging weakened the Al.

1. INTRODUCTION

In modern car manufacturing, most of the weight comes from steel [1]. Due to its strength, steel is widely used to produce the vital parts that form the frame of the vehicle for protection of the passengers when accidents occur.

However, because of the need to improve the fuel efficiency in the cars as well as decrease the greenhouse effects, Aluminum is being used increasingly in the car industry for its lightweight and toughness. It can be used in automotive manufacturing to create body panels for a lighter, more fuel-efficient vehicle. In addition, more automakers are switching from traditional iron blocks for engines to aluminum construction. Aluminum tends to be not quite as durable as iron, but its lighter weight means a big enhancement in performance [2]. Consequently, there is an increasing demand for joining steels and Al alloys in car manufacturing.

Because of the large difference in melting points, it is not possible to weld Al-alloys to steels using conventional fusion welding processes. The TLP process is emerging as a promising technique because it has several advantages: the absence of a heat affected zone, a low heating temperature and compressive pressure, and a low probability of unfavorable reaction [3].

In this work, the TLP technique was used to join 1020 and 304L stainless steels to 6061 Al T-6 alloy using gallium as a filler metal. To evaluate the quality of the bonding, optical metallurgical analysis, scanning electron microscopy analysis, shear testing, and micro-hardness

testing were performed. The effect of different holding time and processing temperature on the bonding property were discussed as well.

2. LITERATURE REVIEW

2.1   <u>Joining Aluminum to Steel</u>

The automotive industry has been making great efforts in reducing the weight of cars based on a need for energy efficiency [4]. One of the most striking innovations is the application of light-weight materials to automotive parts. Materials such as aluminum and magnesium alloys and plastics, including carbon-fiber-reinforced plastic, allow for reduction of car body weight [5]. Of these materials, aluminum alloy seems the most promising because it is both strong and inexpensive [5]. The increasing application of aluminum alloys calls for technology to join aluminum alloy and steel [5].

Various methods have been developed for joining aluminum to steel including fusion welding, solid-state bonding, and brazing [5].

Fusion welding techniques such as arc welding and resistance spot welding are common methods to join materials. However, because of their intensive heat input, in the case of joining aluminum to steel, the formed joints are susceptible to thick brittle intermetallic (IMC) layer [7], heavy cracking [8], and serious porosity [9], resulting in poor mechanical performance.

In contrast, the laser joining is showing a potential of bonding aluminum to steel because of its ability to focus high-energy densities on a small area [10], making it possible to combine short process times and high cooling rates with high joining speeds and thereby limiting the growth of the IMC layer [11].

Friction stir welding (FSW), a traditional solid-sate bonding method for joining aluminum alloys, has been widely applied in the manufacturing industry. Recently, this method has also been applied in joining steels [9-10]. FSW has the advantages of low heat input, less formation of IMCs, and higher weld quality [14]. However, this technique has a few drawbacks. For instance, withdrawing the tool often leaves a hole, heavy-duty clamping is necessary to hold the plates together, the less flexibility with thickness variations and nonlinear welds [15].

The main problem of joining aluminum to steel is the wide difference in the material properties between steel and aluminum that causes the formation of Fe_xAl_y intermetallic compounds [6]. Any joining method that requires high temperatures forms a brittle layer of intermetallic compound (IMC) at the joint interface, which weakens the strength of the joint [5]. Controlling the diffusion and limiting the formation of this brittle IMC layer is therefore vital to overcome this problem.
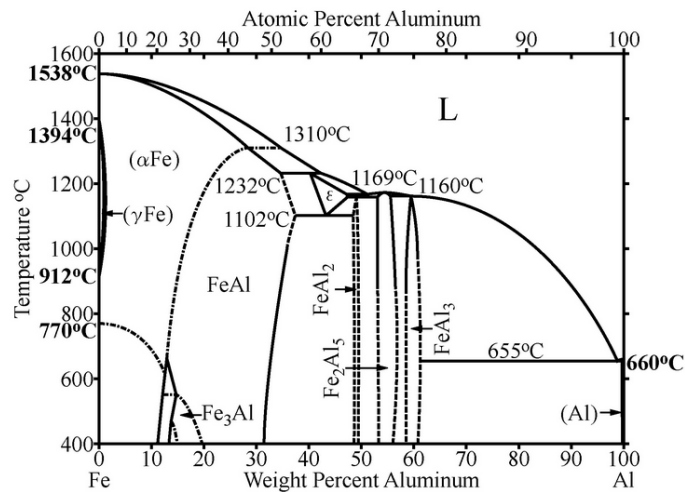
Figure 1. Iron-Aluminum phase diagram [18].

Referring to the Iron-Aluminum phase diagram as shown in Figure 1 [18], several intermetallic compound can be developed, where FeAl and Fe_3Al are considered as ductile phases whereas $FeAl_2$, Fe_2Al_5 and $FeAl_3$ are recognized as brittle phases [16-17] .

2.2 Introduction to TLP Joining

Transient liquid phase (TLP) bonding is a brazing process whereby materials are bonded using an interlayer metal. During heating, the interlayer metal alloys the metal substrates, resulting in localized melting of the newly formed alloy; the temperature is held constant for a period of time, allowing the interlayer element(s) to diffuse into the substrate materials and leading to isothermal solidification because the solute forms a solid solution with the substrates. Ideally, the interlayer alloy diffuses entirely into the substrates, leaving a continuous microstructure between the metals formed. However in most cases a eutectic or a reaction layer interface develops. The fabrication of a TLP bonding involves the following steps [19]:

- Position filler metal between substrates to be joined [19].

- Heat the specimen to the processing temperature, which in most cases is below the melting point of the filler and base metals [19].

- Hold the joint at the bonding temperature until the liquid interface has isothermally solidified [19].

- Homogenize the joint at a suitable heating temperature [19].

2.2.1 Process of TLP Bonding

Tuah-Poku et al. [20] explains the TLP bonding process in a phase diagram (Figure 2) that delineates four stages corresponding to composition regimes.

5

I. Dissolution of base metals with filler metal →

II. Widening of the interlayer →

III. Isothermal solidification →

IV. Homogenization →
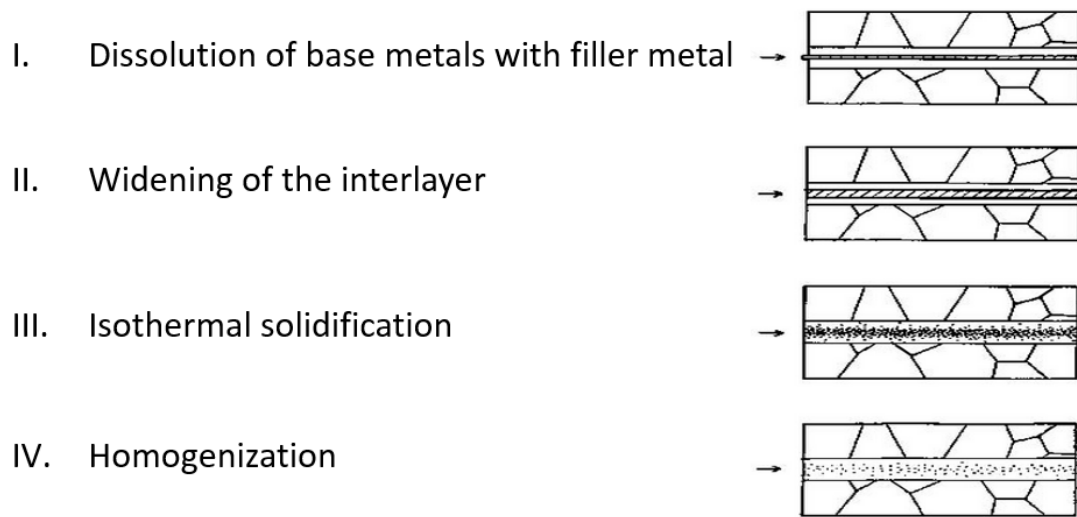
Figure 2. Four stages of TLP bonding process [21].

In their approach, a binary eutectic system was investigated. Figure 3 displays a phase diagram of silver-copper. An interlayer of silver is sandwiched between two copper sheets and the silver is acting as the melting point depressant (MPD) [21]. Upon heating to the bonding temperature (T_b), a liquid phase is formed by the inter-diffusion of silver filler and copper base metal. As the dissolution advances (stage I), the composition of the interface moves from CαS to CαL [21]. Widening (stage II) follows as the interlayer is further diluted into Cu base, and the composition moves from CαL to CβL. In stage III or the isothermal solidification step, as the silver continues to diffuse into the copper, the composition moves from CβL to CβS, and the interlayer begins to narrow. As soon as solidification ends, the concentration of Ag will continue to decrease as holding the joint at the bonding temperature, which results in homogenization, namely the stage IV [21].
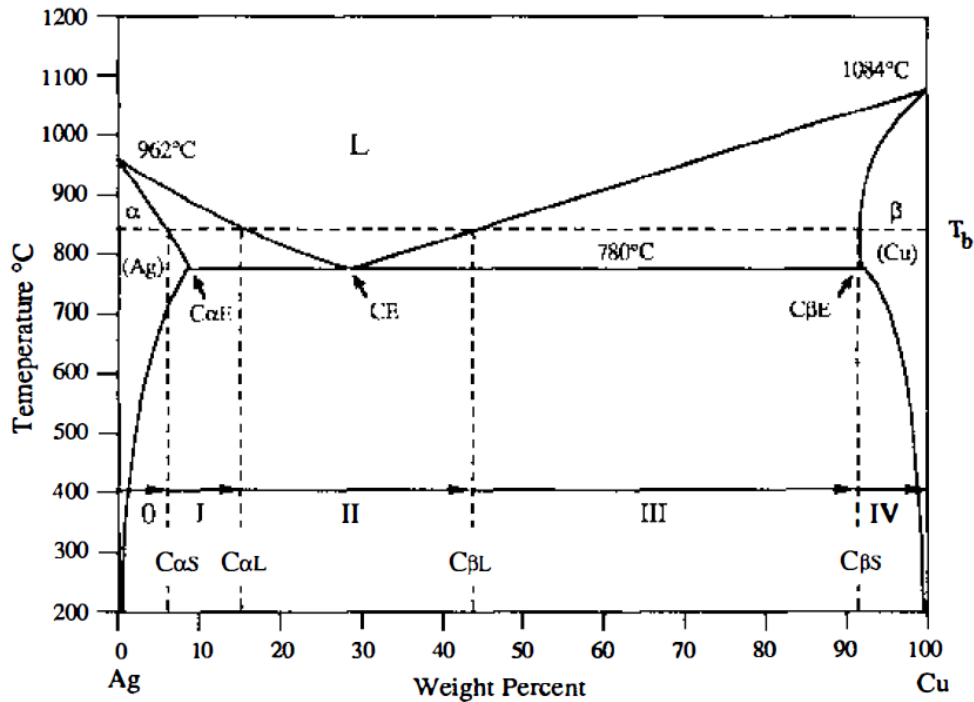
Figure 3. Stages of TLP bonding that occur when silver is bonded with a copper interlayer [21].

The TLP process is not limited to binary eutectics. In this work, a film of Ga is sandwiched between an Al-based alloy and a carbon steel or a stainless steel. Ga act as a melting point depressant to promote the diffusion of the elements in the two base metals. The process is similar to the binary system described above. A liquid interlayer forms from the dissolution of the parent metals and the filler metal. Then, widening of the interlayer occurs as the MPD diffuses further into the base metals. As the Ga continues to diffuse, the interlayer begins to narrow and the isothermal solidification occurs. Maintaining the bonding temperature will continue to decrease the concentration of Ga at the interlayer, which results in homogenization.

2.3   Methods Used in TLP Joining of Dissimilar Materials

H. Umeshita et al. [22] reported the effects of alloying elements on interfacial properties of diffusion bonding of aluminum and steels. In this case, the reaction compounds at the interface were identified as Fe_2Al_5 and $FeAl_3$; the researchers suggested that the growth of these intermetallic layers has a significant effect on mechanical properties of the joints [22]. Joint strength of more than 70 MPa obtained when the average thickness of reaction layers and un-bonded area at the interface were controlled to be less than 1.5 μm and 30%, respectively [22]. The uneven reaction layers in the joint with high carbon steels were responsible for the bonding region's poor mechanical properties.

Masaki Koba et al. [23] studied the joining of magnesium alloy and steel by liquid-phase bonding using silver as the filler metal [23]. In their investigation, eutectic melting and subsequent isothermal solidification occurs on the Mg side where adjacent to the interface of Mg alloy and the inserted silver metal, whereas the thin interface layer formed between the melt and the steel was determined to join the steel to the Mg alloy [23]. A bonding strength of 200 MPa was obtained from the tensile test. They also identified that, the tensile strength of the joint bonded by TLP is much greater than that bonded without a filler metal insert, and even greater than the yield strength of the Mg alloy (in Figure 4) [23].
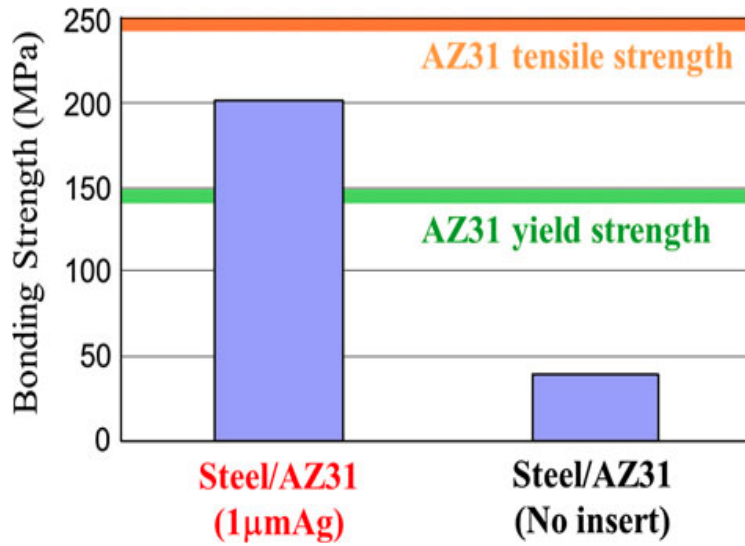
Figure 4. Bonding strengths of steel/AZ31 joints with and without Ag insertion [8].

Wu Ming-fang et al. [24] studied the Al-alloy/Cu/stainless steel joints. Figure 5 shows the image of a specimen bonded at 570°C for 20 min. The researchers observed two reactive layers—(D) and (E)—with 10 um in thickness.

9
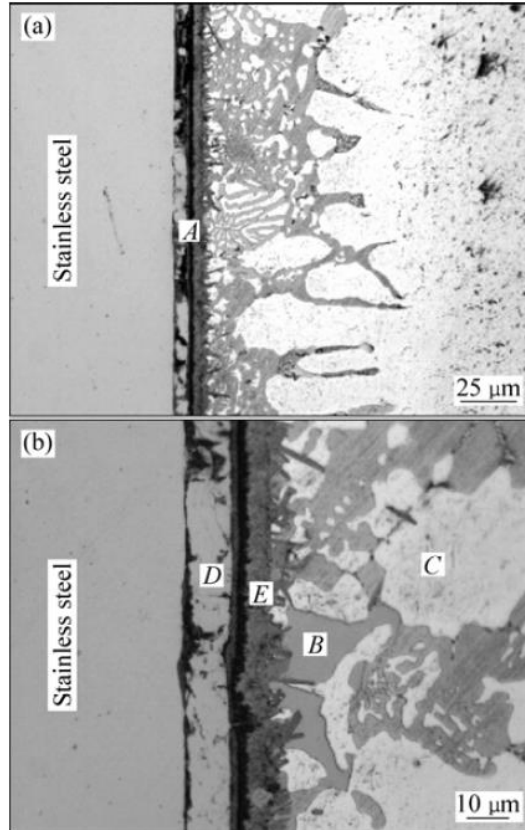
Figure 5. SEM images of sample bonded at 570 °C for 20 minutes (a), and magnified interface microstructure of zone A (b) [24].

The reaction layers near stainless steel side (D) are composed of Fe_2Al_5, $FeAl_3$ and Cu-Al intermetallics, whereas the structure of Cu-Al eutectic with Al solid solution is identified on the Al alloy side (E) [24]. However, the researchers did not report the joint's mechanical properties.

E. Lee et al. [25] developed an innovative process to join Al sheets at moderate temperatures (200–300°C) by combining accumulative roll bonding with transient liquid phase bonding using Ga. Figure 6 shows peeling force versus peeling distance plots for different samples. The higher values of the Ga-coated samples demonstrate the benefit of using Ga in enhancing

bonding between Al strips via transient liquid phase bonding (TLP) brazing. However, the decrease in the 300ºC Al/Ga/Al specimen's peeling strength compared with that of the specimen processed at 200ºC suggests that greater diffusion of Ga into the Al strip when exposed to the higher temperature likely resulted in embrittlement.
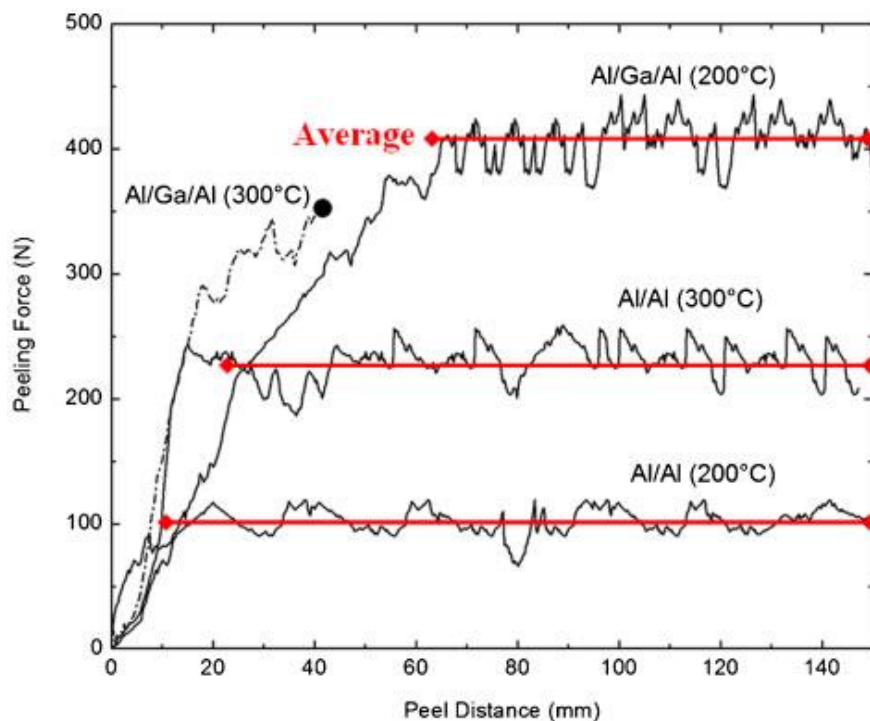
Figure 6. Peel distance versus peeling force [25].

Jun-Yen Uan et al. [26] studied the effects of gallium on metallurgical and physical properties of aluminum alloy 6061-T4. By investigating double-notched samples which applied various amount of Ga, they found that even a small amount of gallium applied on the Al alloy's surface causes a apparent decrease of tensile properties of AA6061-T4 [26]. Increasing the amount

11

of applied Ga (from 3 mg to 5 mg) can seriously weaken the Al because of more embrittlement on the grain boundary [26]. They concluded that, "The inter-granular embrittlement of the aluminum alloy wetted by small amount of Ga involves the combination of two effects: (i) Ga metal on grain boundary embrittlement, and (ii) Ga-induced magnesium enrichment on the grain boundary that further decreases the strength of the grain boundary [26]."

According to the literature, diffusion is directly related to the bonding time and temperature. The reaction layer's thickness also depends on the parameters listed above. No specific criteria were found to determine a relationship between joint strength and reaction layer thickness. Radscheit et al.[26] reported attaining good mechanical properties when the thickness of the intermetallic layer is less than 10 μm in a laser joining of a similar Al-steel system.

In this work, one of the main objective is to establish the optimal parameters. Excessive diffusion resulting from high brazing temperatures and long holding times should be carefully controlled to avoid or limit the growth of an IMC layer. In contrast, short holding times and low bonding temperatures may result in poor bonding.

2.4   Materials

2.4.1   Base Materials

The base materials used in this work are 1020 low carbon steel, 304L stainless steels and 6061-T6 aluminum alloys. Detailed chemical composition and mechanical properties of each are shown in Table I-III [12, 27] .

TABLE I
CHEMICAL COMPOSITION AND MECHANICAL PROPERTIES OF 1020 STEEL [12, 27].

1020 Steel		
Composition	Iron(Fe)	99.08-99.53%
	Carbon(C)	0.18-0.23%
	Manganess(Mn)	0.3-0.6%
	Phosphorus(P)	0.04% max
	Sulfur(S)	0.05% max
Mechanical Properties	UTS	450 MPa
	Yield Strength	330 MPa
	Hardness	B 78/HV 144
	Elongation	10.00%

TABLE II
CHEMICAL COMPOSITION AND MECHANICAL PROPERTIES OF 304L STAINLESS
STEEL [27].

304L Stainless Steel		
Composition	Iron(Fe)	Balance
	Carbon(C)	0.03%
	Manganess(Mn)	2%
	Phosphorus(P)	0.04% max
	Sulfur(S)	0.03% max
	Silicon(Si)	0.75% max
	Chromium(Cr)	18.0-20.0%
	Nickel(Ni)	8.0-12.0%
	Nitrogen(N)	0.10% max
Mechanical Properties	UTS	505 MPa
	Yield Strength	215 MPa
	Hardness	B 80/HV 152
	Elongation	55.00%

TABLE III
CHEMICAL COMPOSITION AND MECHANICAL PROPERTIES OF 6061-T6 ALUMINUM
ALLOY [27].

6061-T6 aluminum alloy		
Chemistry	Aluminum(Al)	95.8-98.6%
	Chromium(Cr)	0.04%
	Mangnesium(Mg)	0.8-1.2%
	copper(Cu)	0.15-0.4%
	Silicon(Si)	0.4-0.8%
	Iron(Fe)	0.7% max
Mechanical Properties	UTS	310 MPa
	Yield Strength	276 MPa
	Hardness	B 60/ HV107
	Elongation	12.00%

2.4.2   Filler Metal

Gallium was used as a filler metal and melting point depressant in this investigation. A thin layer of gallium was brushed on the each surface of the metal substrates. When the filler metal is heated above its melting point (T_M = 29.7°C), the liquid Ga will react with the base metals and form a liquid alloy at the bonding region. This liquid alloy will later isothermally solidify during holding at the bonding temperature because of the diffusion of Ga, Al, and Fe across the bonding interface.

Phase diagrams of Iron-Gallium and Aluminum-Gallium are shown in Figure 7-8 [28, 29]. It is possible to form a liquid phase in the interlayer at a bonding temperature well below the melting points of both the base metals.
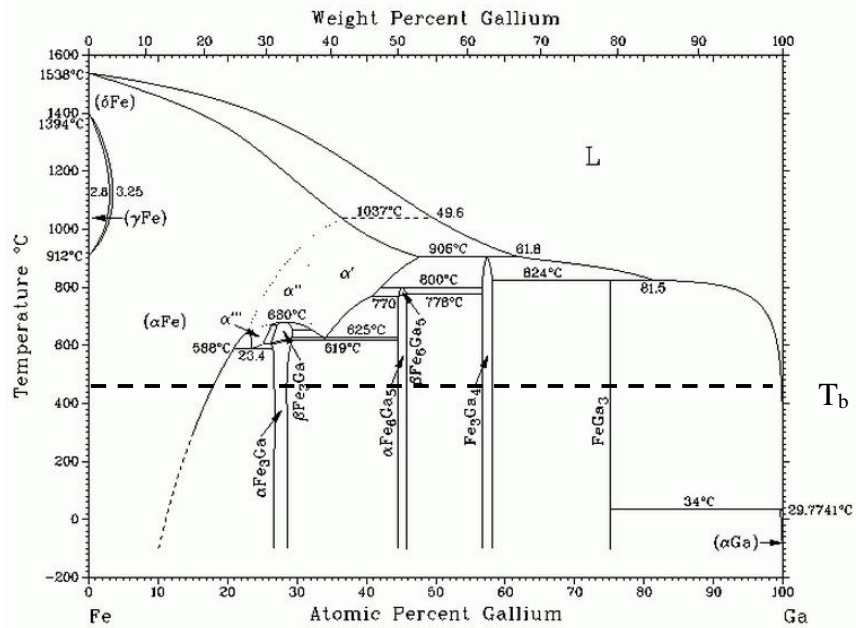
Figure 7. Iron-Gallium phase diagram [28].
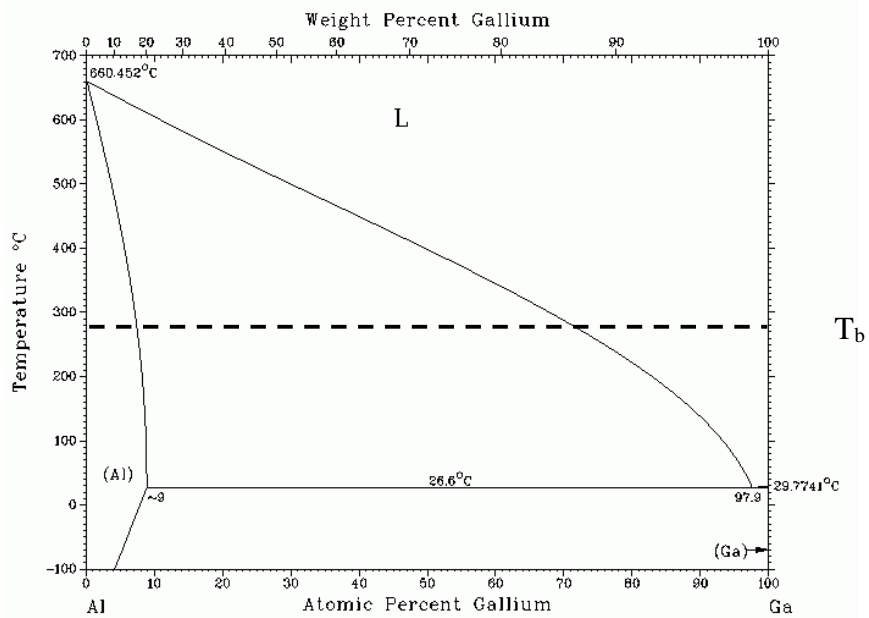
Figure 8. Aluminum-Gallium phase diagram [29].

15

2.5   Welding of 6061-T6 Aluminum Alloy

6061-T6 is a precipitation-hardened aluminum alloy whose major alloying elements are magnesium and silicon . T6 temper 6061 has an ultimate tensile strength of at least 300 MPa and a yield strength of at least 240 MPa [30]. Because of its relative low density and high strength, 6061 Al is widely used in constructing aircraft structures, automotive parts, bicycle frames, and so forth. However, during the welding processes, a large heat input is transferred into the base material through heat conduction. This non-uniform thermal dissipation will lead to localized isothermal sections which has an important and detrimental effect on the microstructure and mechanical properties of the heat-affected zone (HAZ) [31], causing the alloy to be overaged and the joint to soften and weaken. This microstructural change affects the welded joints' in-service performance because the mechanical properties of the HAZ are reduced drastically with respect to base material [31].

One challenge in this work is to minimize the damage caused by heating on mechanical properties of 6061 Al-T6. Using the TLP process, joining can be performed at very low temperatures (330–480°C).

3. EXPERIMENTAL PROCEDURE

3.1   Technical Approach

The goal of this work is to develop a metallurgical understanding of joining two dissimilar metals via Transient Liquid Phase (TLP) bonding; and to establish the optimal parameters for bonding 1020 carbon steel and 304L stainless steels to 6061 aluminum alloy. According to the literature review, the bonding temperature and holding time and the usage of filler metal will have a significant effect on the bonding properties. To understand those effects, two types of braze joints were fabricated: (i) 1020 steel to 6061Al-T6 and (ii) 304L stainless steel to 6061 Al-T6 samples. In addition, a control set of samples were fabricated with no filler metal at each of the bonding temperatures and holding times. An inert gas atmosphere was applied during heating using a tube furnace. Joint strength was investigated by means of a lap-shear test to evaluate the bonding strength, and a series of metallurgical characterizations (optical microscopy and SEM analysis) was performed on samples of interest, including micro-hardness testing across the bonding line.

3.2   Experimental Set-up

Figure 9 shows the equipment setup used in the joint fabrication, including a Lindberg tube furnace and a delivery Ar-gas line with a pressure of 50 psi maintained during heating. The heating temperature was controlled by a heating controller and monitored with an external thermocouple.

Figure 9. Heat treating equipment.
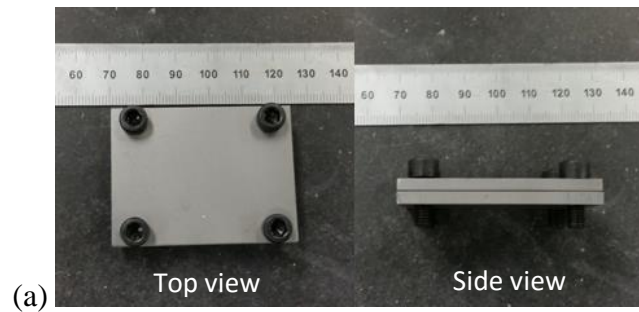
(a)
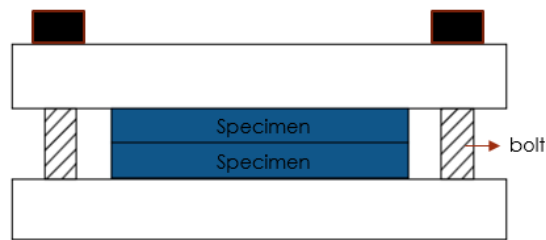
(b)

Figure 10. Clamp designed to frabricate specimen (a) top and side view and (b) schematic of the cross section view of the whole assembly.

Figure 10 shows a steel clamp holder used for the fabrication of the joints. Five newton·meter (N·m) of torque was applied on each bolt to impose uniform pressure on every specimen.

3.3   Fabrication of TLP Joined Specimens

For metallographic studies, the materials were machined into rectangular shaped samples (25.4×12.7×1.58 mm) as shown in Figure 11. Before joining, the faying surfaces were grounded to 1200 grit and cleaned with Acetone. The two pieces of base metals were preheated to 80°C to promote spreading. Ga liquid film was then spread uniformly on both surfaces of the base metal samples. Both base metals with Ga were placed in contact and clamped into the braze assembly (Figure 10). The whole assembly was introduced in the tube furnace. The furnace was then purged with Ar-gas prior to heating. Then, the samples were exposed to the heating cycles, as shown in Figure 12. The detailed fabrication matrix is listed in Table IV.
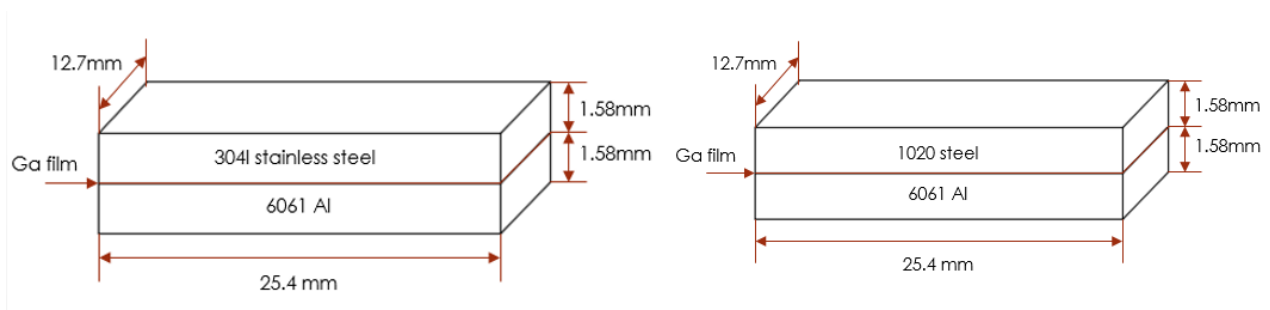
Figure 11. Dimensions of bonding systems.
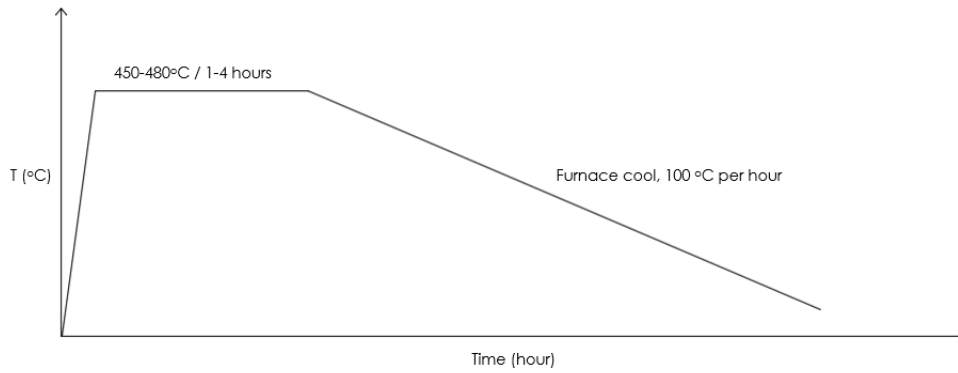
(a)
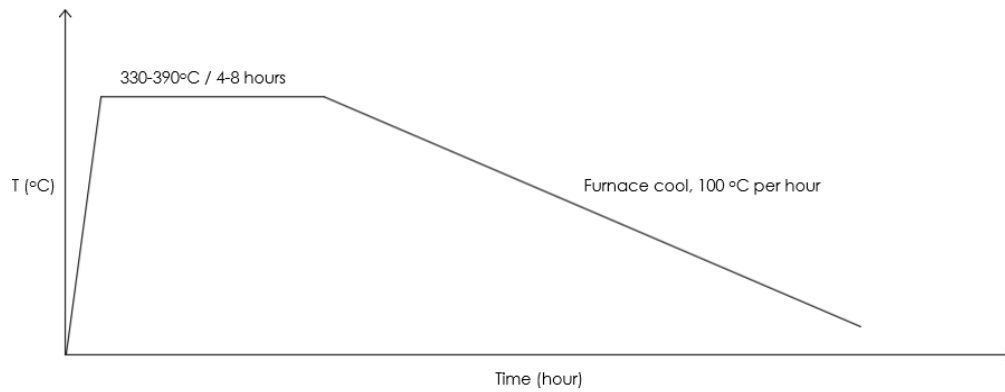
(b)

Figure 12. Heating cycles for (a) 1020 steel/6061 Al-T6 system, (b) 304L SS/6061-T6 system.

TABLE IV
SAMPLE FABRICATION MATRIX

Joining system	Holding temperature(^{o}C)	Holding time(hours)		
1020 Steel/Ga/6061 Al	450	1	2	4
	480	1	2	4
304L/Ga/6061 Al	330	4	6	8
	360	4	6	8
	390	4	6	8

3.4   Optical Microscopy

After brazing, the joined specimen were sectioned and mounted in epoxy (shown in Figure 13) for metallurgical observations and micro-hardness testing. Samples were grounded using silicon carbide abrasive paper up to 1200 grit and then polished using an alumina suspension up to 0.05 μm. After the joints were ultrasonically cleaned, the samples were etched in different solutions to reveal the reaction layer on each side of the base metals: 2% Nital for the 1020/Ga/6061 Al-T6 specimens, and for the 304L/Ga/6061 Al-T6 joints, Vilella's [32] (2gr Picric Acid + 5cc HCl +100cc Ethanol) and Glyceregia [32] (15cc HCl + 10cc Glycerol + 5cc HNO_3) were used.
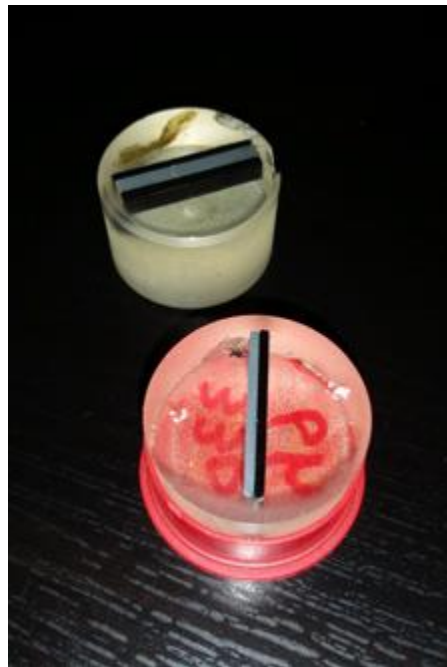
Figure 13. Mounted samples for metallurgical analysis.

3.5   Scanning Electron Microscopy (SEM) Analysis

The instrument used for this portion of the investigation was an Oxford Model 6427 SEM (Figure 14). In addition to the microstructure characterization, SEM/EDS analysis were carried out on selected samples to study the inter-diffusion of Al and Fe and the diffusion of Ga into both substrates as well as to investigate possible chemical reactions near the joint.

Figure 14. Oxford Mode 6427 scanning electron microscope.

3.6   Micro-hardness Measurements

Micro-hardness measurements were conducted across the TLP joint to establish whether intermetallics formed as a result of the Al and Fe inter-diffusion as well as to determine the possible

overage damage of the Al alloy because of the brazing temperature used. A load of 50 (grams·f) was applied. The equipment used was a Leco M400 micro-hardness tester (shown in Figure 15).

Figure 15. Leco M400 micro-hardness tester.

3.7   Tensile Testing

Shear tensile tests were performed according to ASTM 1002 D standard; the test specimens fabricated for the tensile tests had the following dimensions: $101.6 \times 25.4 \times 1.58$ mm. The specimens were bonded with an overlap of 12.7 mm (Figure 17). An MTS model 1125 tensile machine (Figure 16) was used with a crosshead speed of 0.05 in/min; the specimens were pulled to failure.

Figure 16. MTS model 1125 tensile tester.
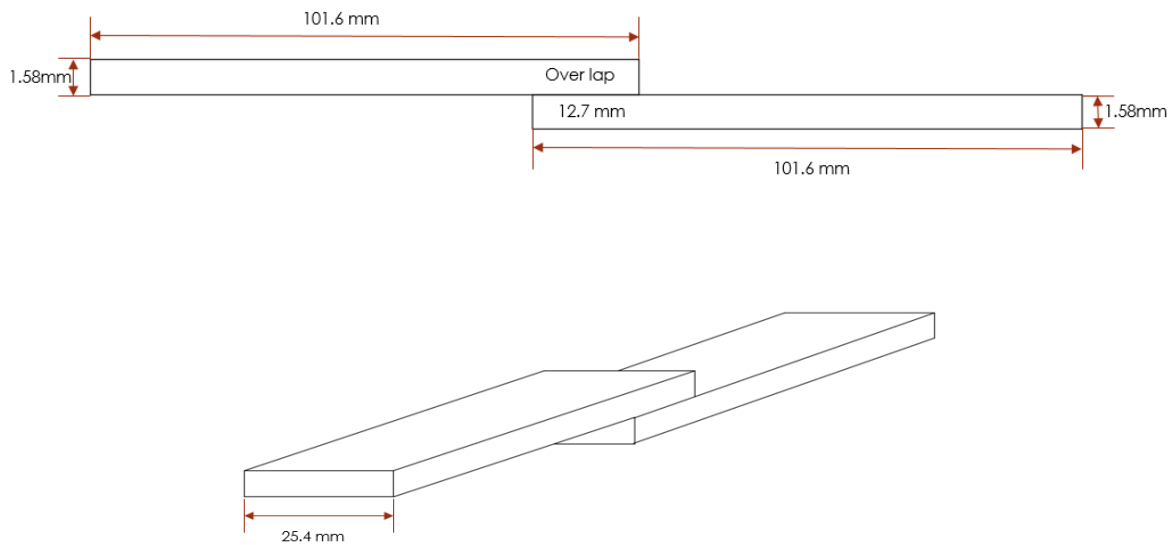
Figure 17. Bonded specimen for tensile testing.

4. RESULTS AND DISCUSSION

4.1   Metallurgical Examinations of the 1020 Steel/Ga/6061 Al-T6 TLP Joints

Metallurgical analyses were performed on all the bonded samples following their fabrication. As indicated in the previous chapter, the cross sections of the samples were metallographically analyzed. In addition, the SEM/EDS analyses were undertaken and the results are discussed below.

4.1.1   Optical Microscopy of the TLP Joints

In the 1020 steel/6061 Al-T6 system, bonds were obtained for those samples fabricated at 450ºC and 480ºC for heating times of one, two, and four hours. Figure 18 and 20 show the bond cross section of the reaction layers of samples bonded at 480ºC and 450°C respectively. It is observed that as the brazing time increases, the reaction layers become wider and more uniform. Several measurements of the width of each sample were made and an average value was obtained as function of the holding time. It was also found that the joints became more brittle with longer bonding, particularly in the specimen fabricated at 480°C for hours, as a crack was found in the middle of the reaction layer (Figure 18c). But no cracks were detected in the joints produced at 450°C. Note that joint widths of the 480°C specimens were wider, as expected, because of the higher temperatures that favor a greater diffusion.
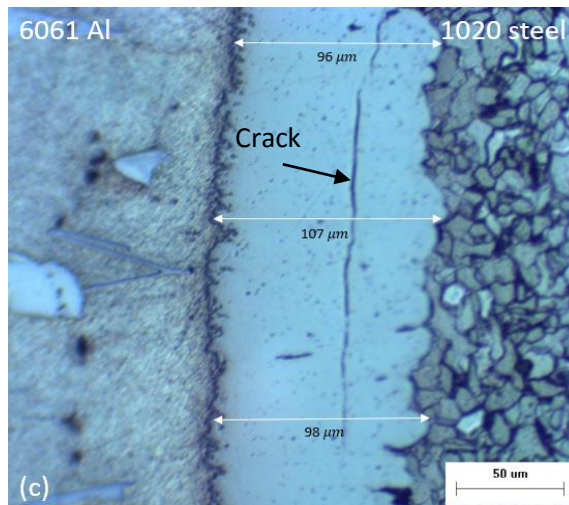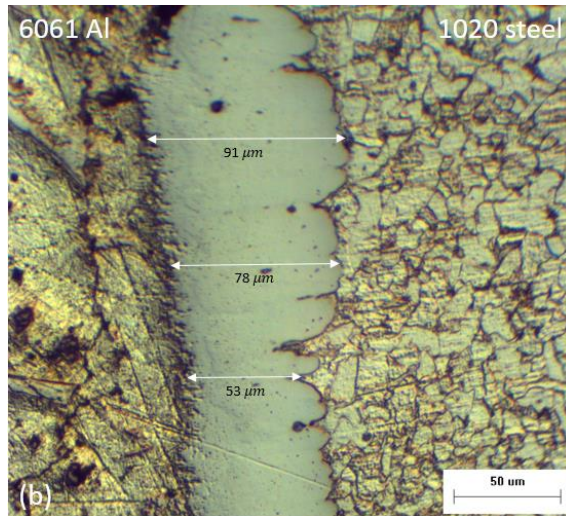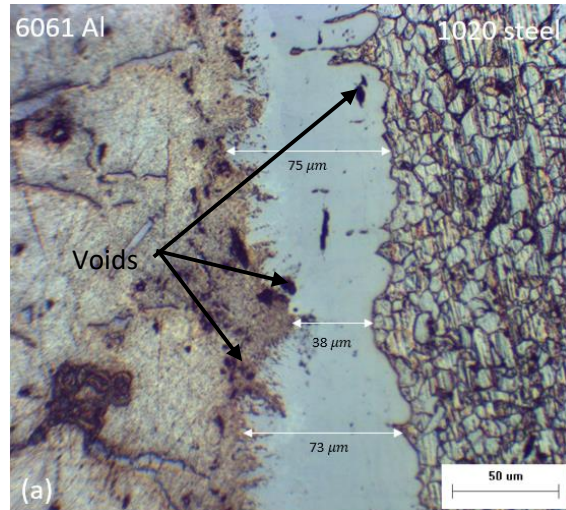
Figure 18. Reaction layers of 1020 steel/Ga/6061 Al specimen bonded at 480°C: (a) hold for one hour, (b) hold for two hours, and (c) hold for four hours.
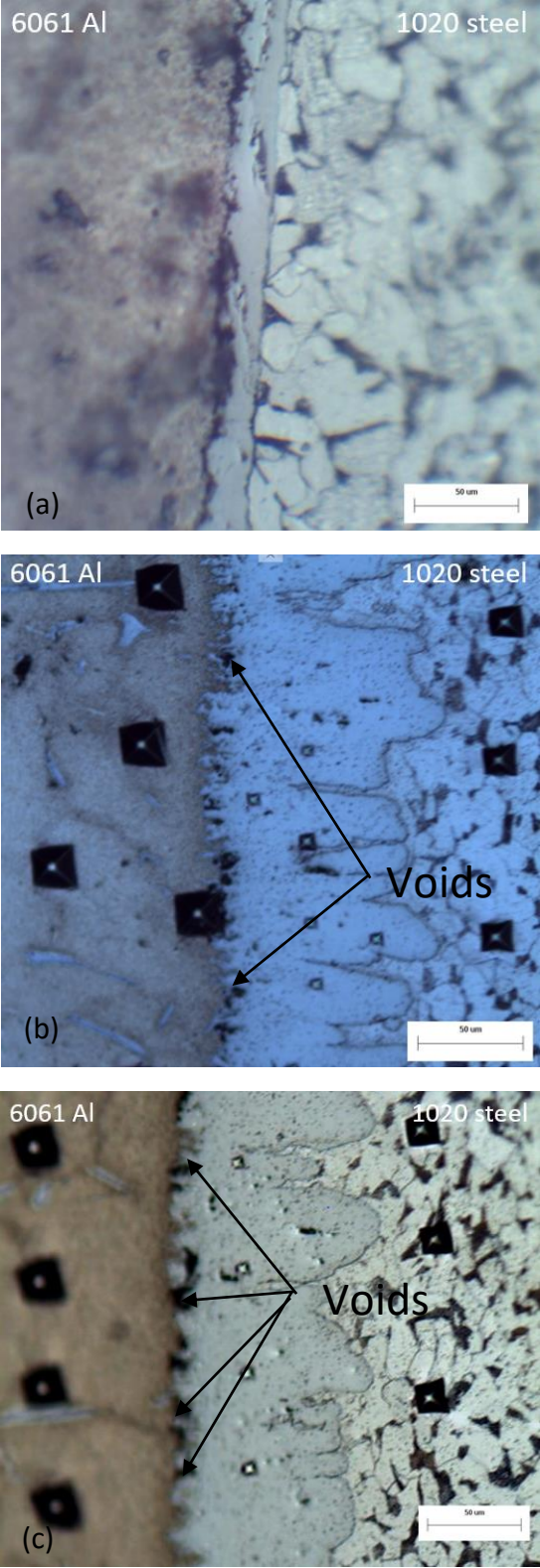
Figure 19. Reaction layers of 1020 steel/Ga/6061 Al specimen bonded at 450°C: (a) hold for one hour, (b) hold for two hours, and (c) hold for four hours.
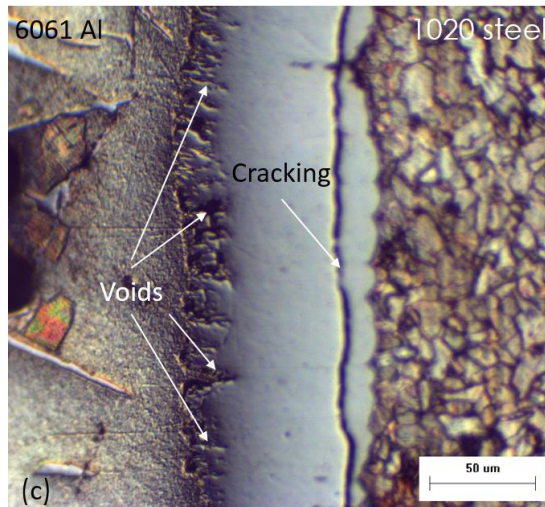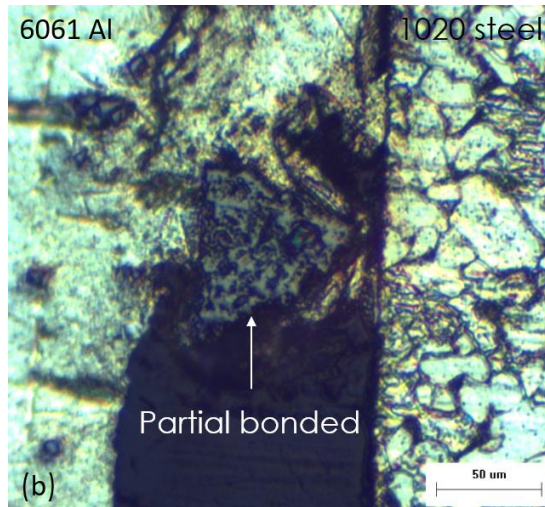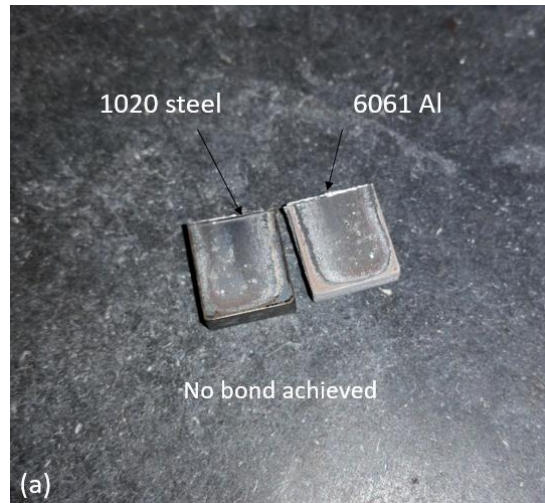
Figure 20. Reaction layers of 1020/no Ga/6061 Al joints bonded at 480ºC without applying Ga:
(a) hold for one hour, (b) hold for two hours, and (c) hold for four hours.

As mentioned above, the embrittlement of the reaction was first recognized by the development of a crack along the reaction layer (Figure 18c). The composition of this reaction layer was identified by means of SEM/EDS as brittle intermetallic Fe_2Al_5. Details on the SEM analysis are presented at a later section. It is also apparent that the reaction layer formed mostly on the steel side because Al diffused extensively into the steel.

A control group of 1020 steel/6061-T6 joints with no Ga deposited was produced for the purpose of studying the effect of Ga on the diffusion of Al and Fe. The samples were fabricated at 480°C using the same holding times. The corresponding micrographs for the joints fabricated with no Ga are shown in Figure 20. No bonding resulted for the sample produced at the one-hour holding time (Figure 20a), whereas partial and poor bonding was obtained for the sample exposed to two-hour holding time (Figure 20b).

In Figure 19c, a long and deep crack near the reaction layer centerline was detected for the control sample bonded at 480°C for four hours. A significant number of voids were observed at the interface of reaction layer and 6061 Al. According to the metallurgical photographs, the bondings processed without Ga appear to be weaker and more defective than the ones bonded with Ga.

A bond developed in the specimen fabricated at 480°C with no Ga, as seen in Figure 20c. It is seen that the reaction layer is much narrower than their counterpart produced with Ga; furthermore, a long and deep crack also occurred in the reaction layer centerline. A significant number of voids were also observed between the interface of reaction layer and the 6061 Al-T6.

These results show the beneficial role of Ga in facilitating the bonding between these two dissimilar metals at very low temperatures. Ga also facilitates the formation of the reaction layer by enhancing the diffusion of Al and Fe across the faying surface.

All joint cross sections' reaction layer width measurements are plotted in Figure 21. These results reflect the effect of the processing parameters on the joint width and the benefit of Ga. It is also important to recognize the fact that Ga can cause liquid metal embrittlement of Al, if used in excessive amounts.

As shown in Figure 19, for the 1020 steel/Ga/6061 Al joints bonded at 450°C, as the holding time increases, the width of reaction layers increases as well. Voids were also observed at the interface between the reaction layer and 6061 Al-T6 base metal as the holding time increased.

In addition to the formation of intermetallics, cracking appears to form on a wider reaction layer which is fabricated at a longer holding time, because the solidification will first take place on the zones near each base metals; as the temperature is lowered, the metal at these locations solidifies and contracts, whereas the centerline region will still contain remaining liquid leading to some form of hot crack. Brittle intermetallics appears to precipitate in that region as well. The centerline region in a wider reaction layer can be more vulnerable to cracking and voids because more tension can build up there during solidification because of the shrinkage on its both sides.
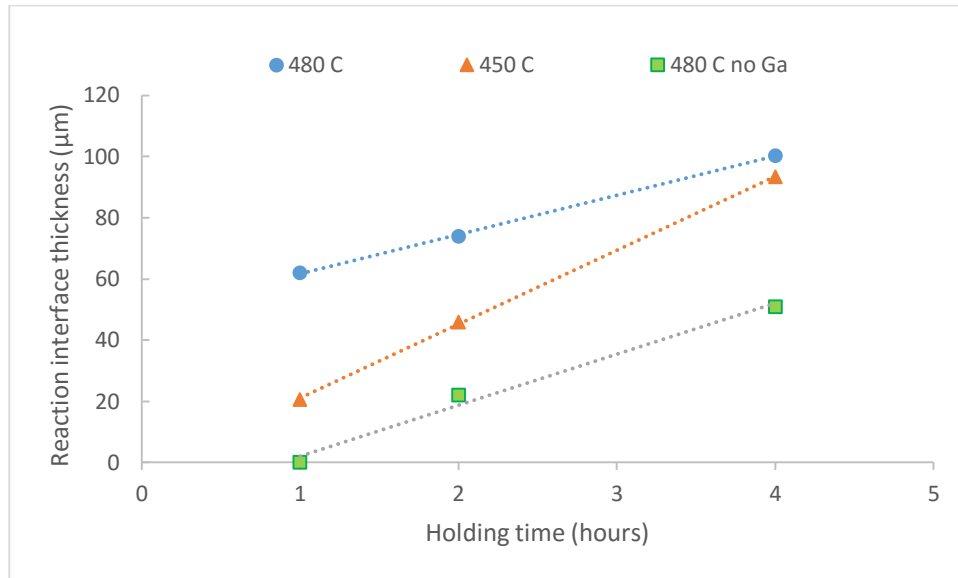
Figure 21. Width of reaction layers of three sets of samples as a function of holding time.

4.1.2 SEM/EDS Analysis of the TLP Joints

An SEM evaluation was conducted of the TLP joint produced at 450°C for a holding time of four hours. The SEM micrograph, shown in Figure 22, presents a middle light reaction layer about 80 μm wide that seems to extend into the 1020 steel. The reaction layer consists of the intermetallic compound Fe_2Al_5, and it appears to have a very tight bond with both substrates. On the Al side of the joint, some discontinuous and dispersed elongated particles, which are iron-rich zones, were observed using electron dispersive spectroscopy (EDS) analysis.
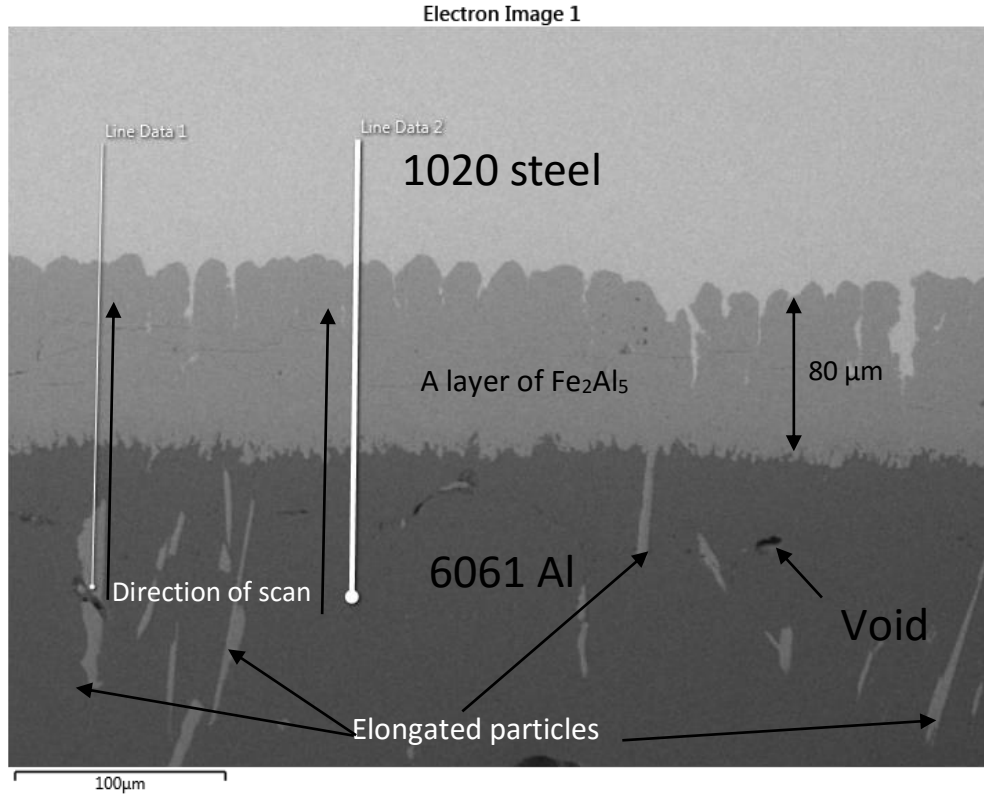
Figure 22. SEM image of joint 1020 steel/Ga/6061 Al bonded at 450ºC for four hours.

Two line scans were performed on this specimen. Line 1 scans from a Fe rich zone in the 6061 Al base through the reaction layer into the 1020 steel base. The direction is the same as line 1 for line 2, but line 1 did not pass the Fe rich zone. As can be seen in Figure 23 (a), in the elongated particle, a higher Fe signal count and lower Al signal count were observed, confirming that those Fe-rich zones are formed by Fe migration. IMC $FeAl_3$ was also identified in this particle.

As can be seen in Figure 23(b), line 2 scans from 6061 Al base to the 1020 base. The redistribution of elements suggests that Fe diffuses into the 6061 Al base and that Al diffuses into the 1020 base. The different chemical composition confirms a reaction layer of width of

approximately 80 μm. The distinct decrease of Al signal and increase of Fe signal also reveals the

boundaries of isothermal solidification zones and base metals.
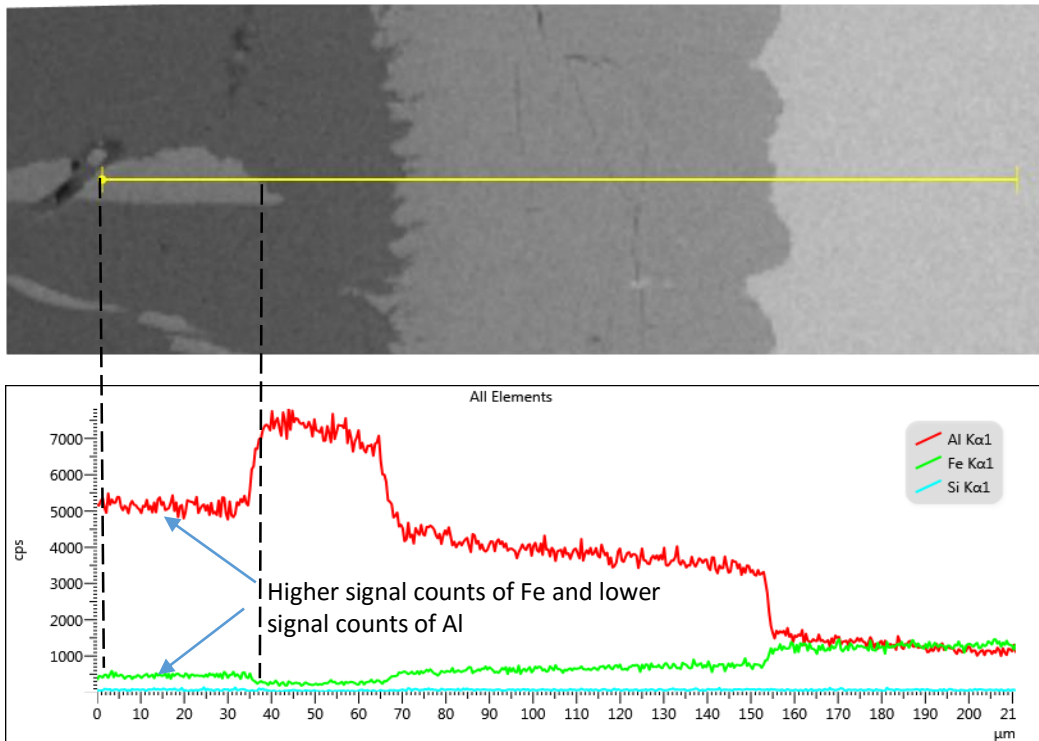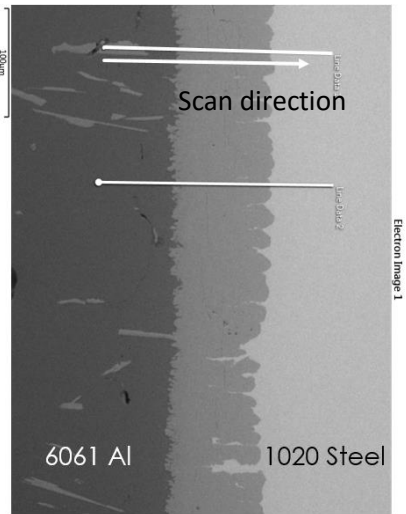
(a) Line scan 1
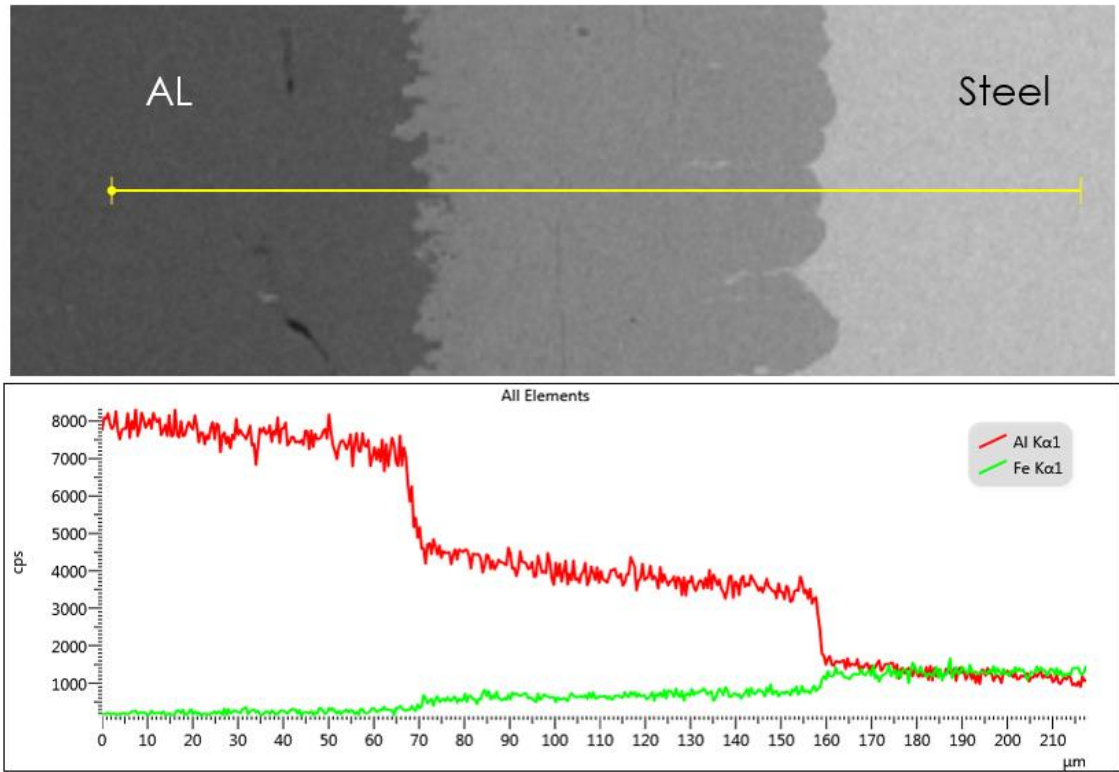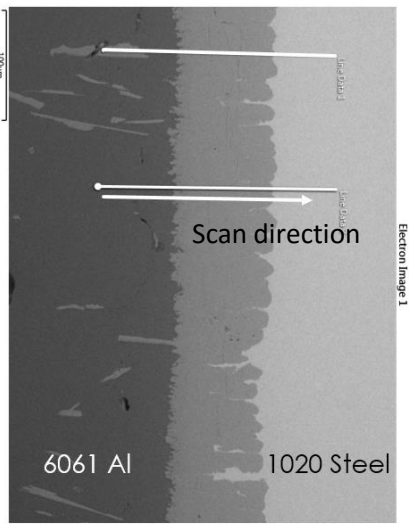
(b) Line scan 2
Figure 23. A comparison of (a) line scan 1 and (b) line scan 2.

According to Fe-Al phase diagram (Figure 24), possible reactions are listed in Table V; in this test, brittle IMC Fe_2Al_5, $FeAl_3$, and ductile IMC FeAl were observed by means of the EDS analysis.
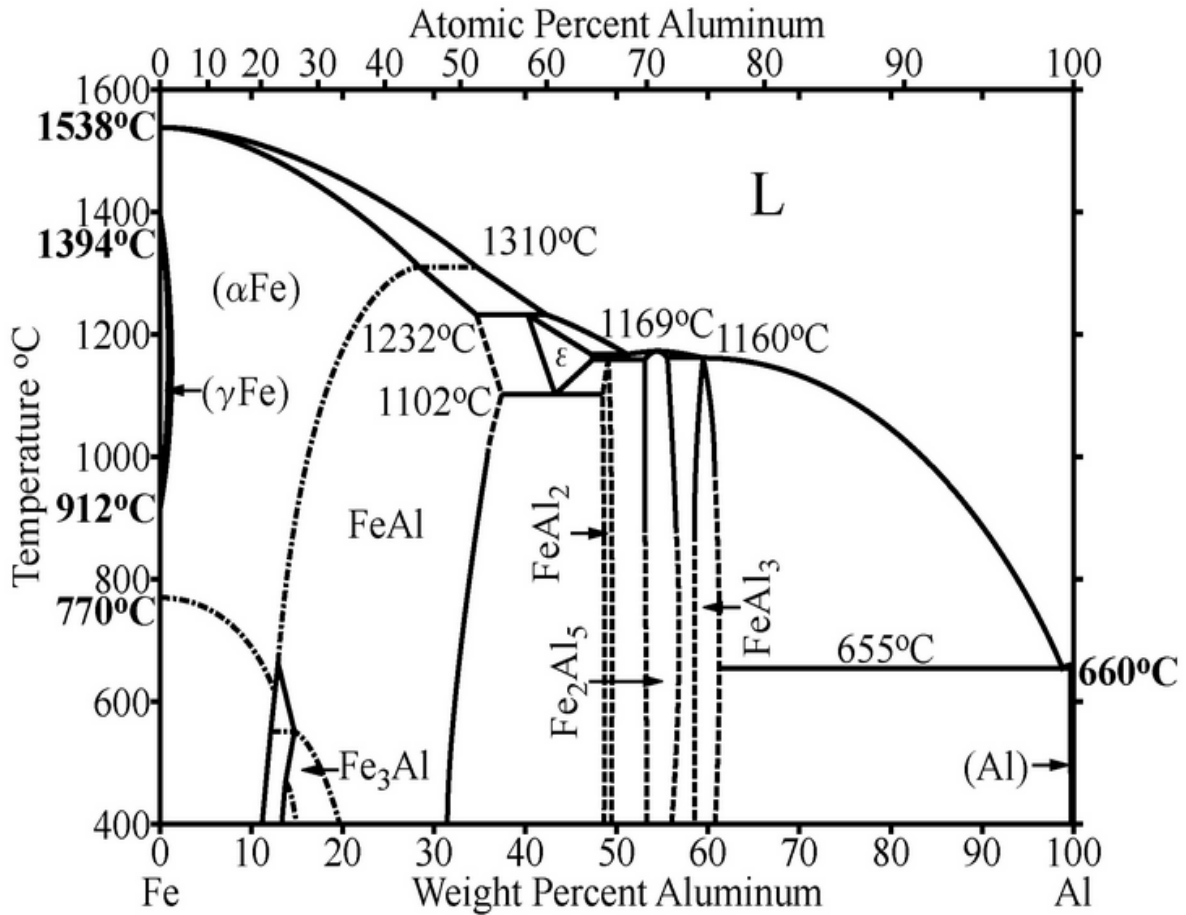
Figure 24. Fe-Al phase diagram [18].

TABLE V.
POSSIBLE REACTIONS AT 1020/6061 Al INTERFACE.

Possible reactions
Fe + Al — FeAl
Fe + Al — FeAl$_2$
Fe + Al — FeAl$_3$
Fe + Al — Fe$_2$Al$_5$
Fe + Al — Fe$_3$Al

Chemical composition analysis was performed on four points on the reaction layer. As shown in Figure 25, intermetallic compound Fe$_2$Al$_5$ (spectrum 1) was confirmed in the middle of the reaction layer. Ductile IMC FeAl (spectrum 2) was identified on the 1020 steel side adjacent to the reaction layer. Brittle IMC FeAl$_3$ (spectrum 4) was identified in the particle on the 6061 Al side.
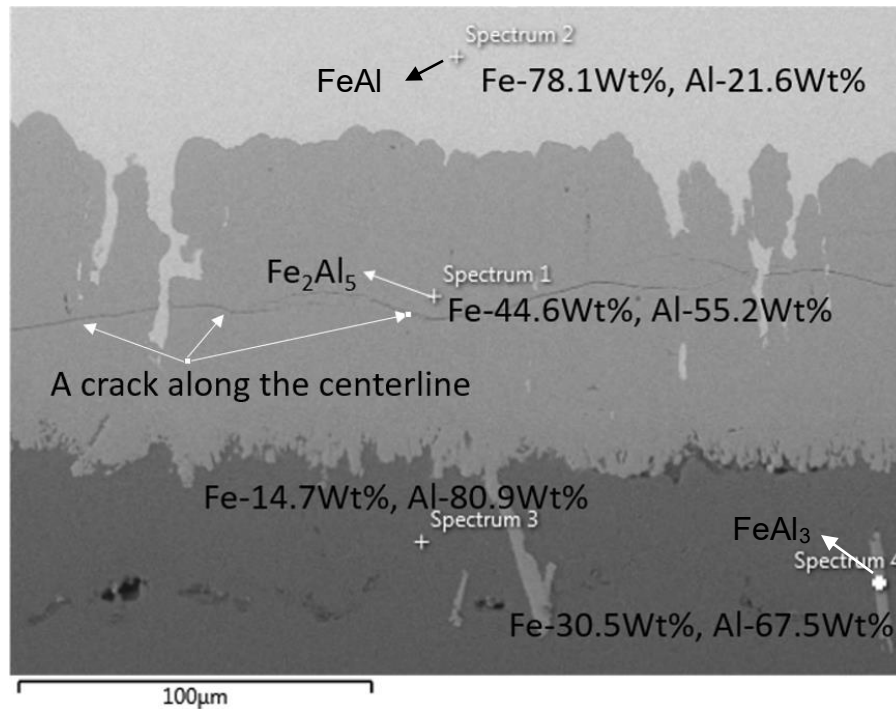
Figure 25. Spectrums used for chemical composition analysis on the 1020 steel/Ga/6061 Al sample bonded at 450°C for four hours.

The control sample prepared to study the effect of filler metal on the diffusion near the bonding region was also analyzed in the SEM, and chemical analysis via EDS was performed. Figure 26 shows the sample bonded at the same holding time and temperature (450°C for four hours) without spreading Ga as filler metal. The SEM image and X-ray mapping indicate a much narrower (about 5 μm versus 80-100 μm width of sample using Ga) and less uniform reaction layer. A line scan (Figure 27) was conducted across the bonding region as well; the diffusion of elements Al and Fe are limited within a range of 5 μm adjacent to the centerline. Less diffusion resulted in a weaker bond: when the joint was sectioned for observation, half of it split apart.
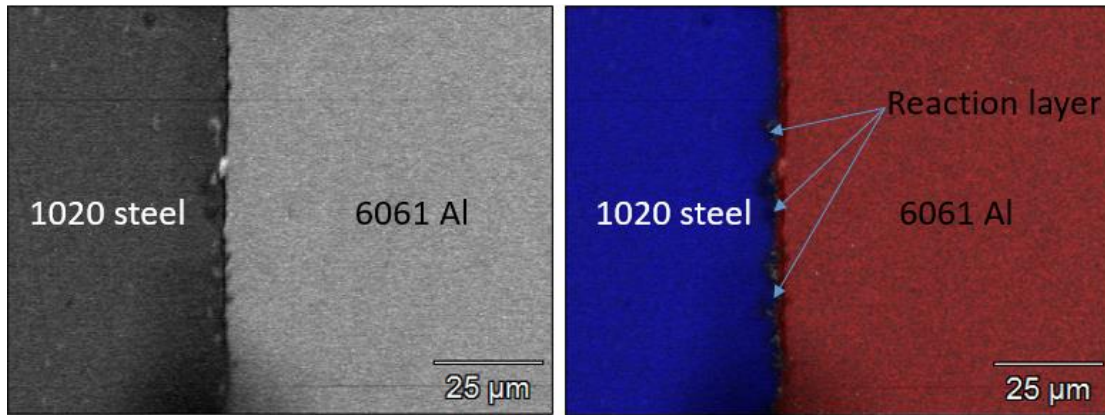
Figure 26. SEM image and X-ray mapping for sample bonded at 450 °C for four hours without spreading Ga.
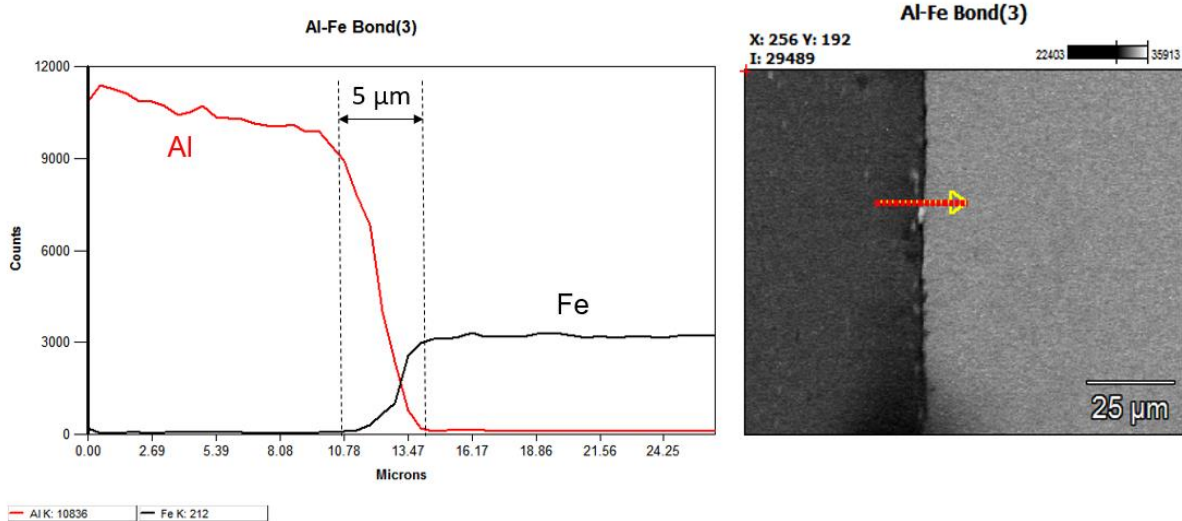
Figure 27. Line scan of 1020 steel/no Ga/6061 Al-T6 TLP joint bonded at 450 °C for four hours.

Diffusion coefficients of both Al in Fe and Fe in Al were roughly estimated from data received, using the solution to Fick's second law assuming constant surface concentrations for each of the elements [33]. The results from samples bonded with Ga and without Ga are compared

in Table VI. For the sample bonded with Ga, diffusion coefficients of both Al in Fe and Fe in Al with Ga are three orders higher than the diffusion coefficients for those without Ga. These rough calculations further describe the significant role of Ga enhancing the diffusion of Al and Fe.

TABLE VI
ESTIMATED DIFFUSION COEFFICIENT OF SAMPLES BONDED WITH AND WITHOUT GA AT 450 ^{O}C FOR FOUR HOURS

1020/Ga/6061 at 450ºC for 4hours	D (m^2/s)
Fe in 6061 Al	1.70E-13
Al in 1020 steel	2.20E-13
1020/6061 at 450ºC for 4hours	D (m^2/s)
Fe in 6061 Al	5.60E-16
Al in 1020 steel	4.20E-16

4.2   Metallurgical Evaluations of the 304L/Ga/6061 Al-T6 TLP Joints

4.2.1   Optical Microscopy of the TLP Joints

For the 304L/Ga/6061 system, no reaction layers were readily detected of the sample (bonded at 330ºC for 6 hours) shown in Figure 28a. No dense reaction layer was identified. Limited reaction was observed in the 304L SS side (Figure 28a), In the case of samples fabricated at 360 and 390 ºC for four hours, the information from the optical microscope did not show any real reaction layer. It appears that the Ga stay near the faying interface in the Al alloy side. The layer also appears porous as shown in Figure 28b-c. Thus a more extensive evaluation using scanning electron microscope is necessary.
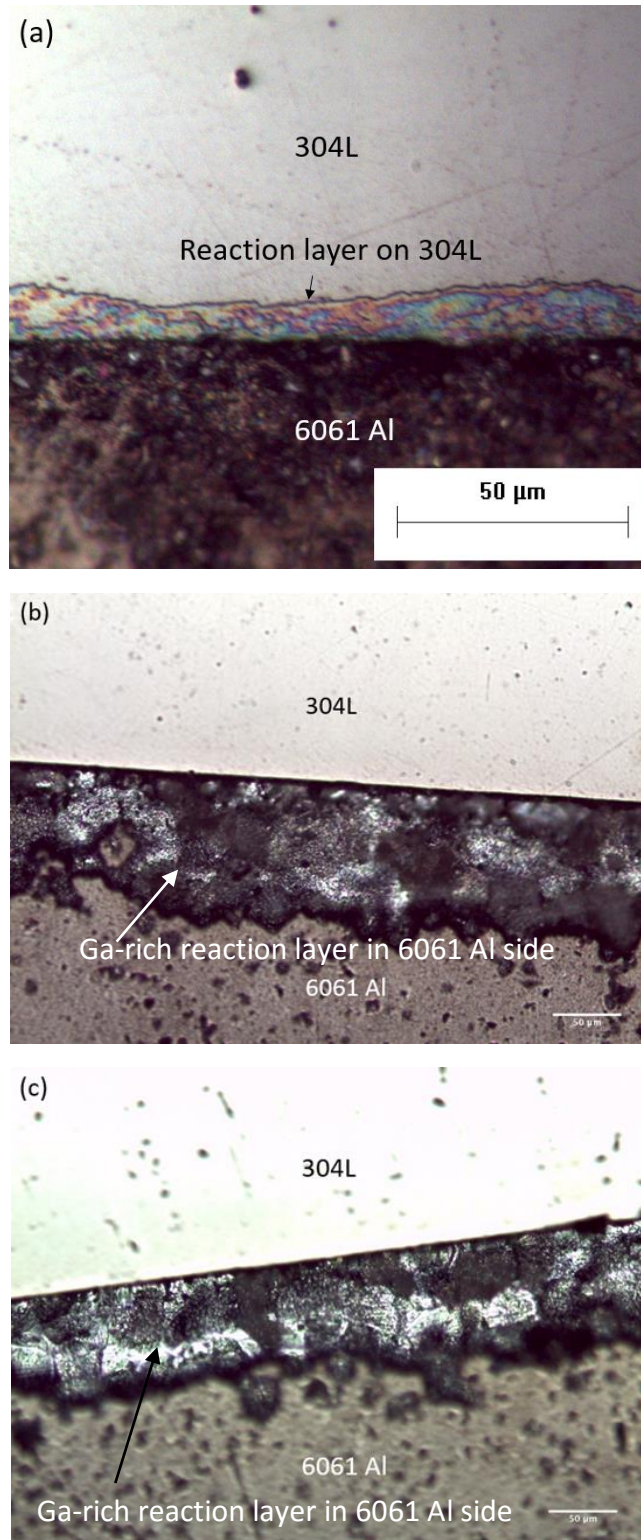
Figure 28. Images of reaction layers of 304L SS/Ga/6061 Al samples: (a) bonded at 330°C for six hours, (b) bonded at 360°C for four hours, and (c) bond at 390°C for four hours.

4.2.2 SEM/EDS Analysis of the TLP Joints

For 304L/Ga/6061 Al system, a sample bonded at 330ºC for six hours was examined. In the SEM image, Figure 29 shows a light and dispersive reaction layer located in the 6061 Al side, with a width that varies between 50 and 100 μm. There is no evidence of any diffusion of Ga or Al into the stainless steel. Line scan to find out the inter-diffusion of Ga, Fe, Al, Cr, and Ni near the bonding region is discussed in the following paragraph.
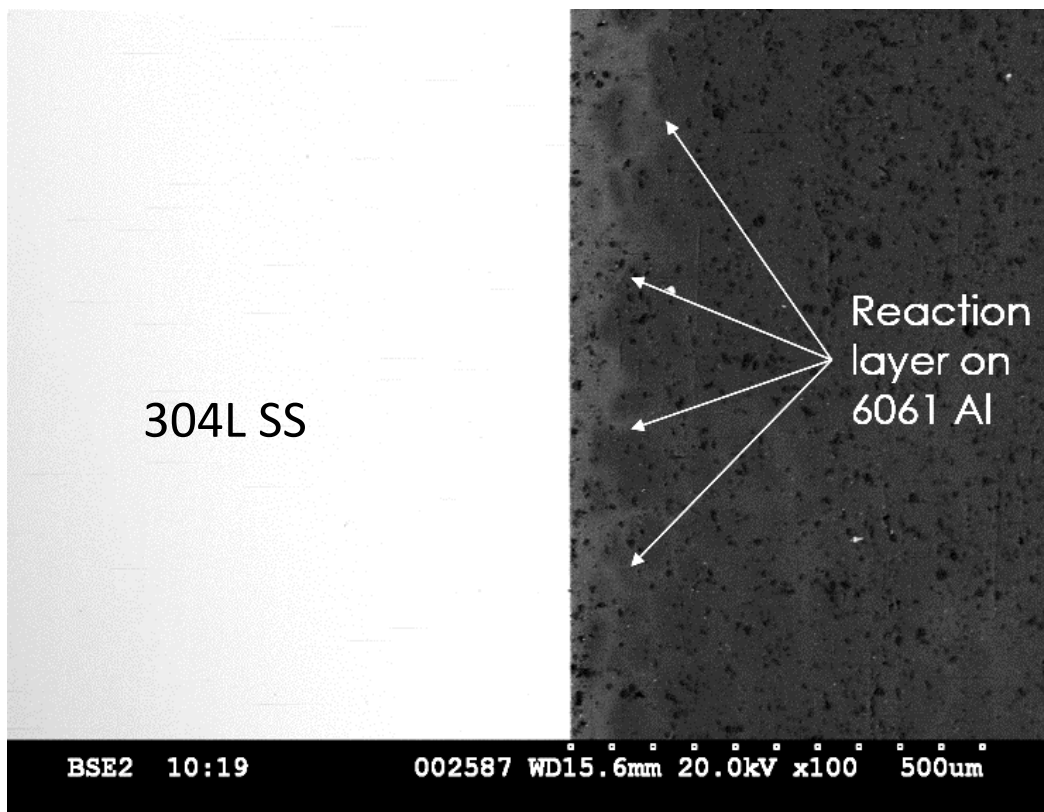
Figure 29. SEM image of joint 304L SS/Ga/6061 Al bonded at 330ºC for six hours.

Two line scans were obtained as shown in Figure 30: both the lines scan from 304L SS to 6061 Al. For line 1, 87 µm in length, the scan covers a wider range on the reaction zone of 6061 Al. As for line 2, 43 µm in length, the scan focuses on the bonding region.

As shown in Figure 30, it was observed that Fe and Cr diffused into the 6061 Al equally. Al also diffused into the 304L base. The migration of Fe and Cr into the aluminum alloy was very narrow, the depth was estimated to be nine to 10 µm. Higher Ga diffusion into the 6061 Al side was detected, and the depth was estimated to be 50 to 100 µm. The line scans showed that the penetration of Ga into the 6061 Al T-6 is not uniform; and the penetration of Al and Ga into the 304L SS is much localized to the bond region (about five µm penetration).
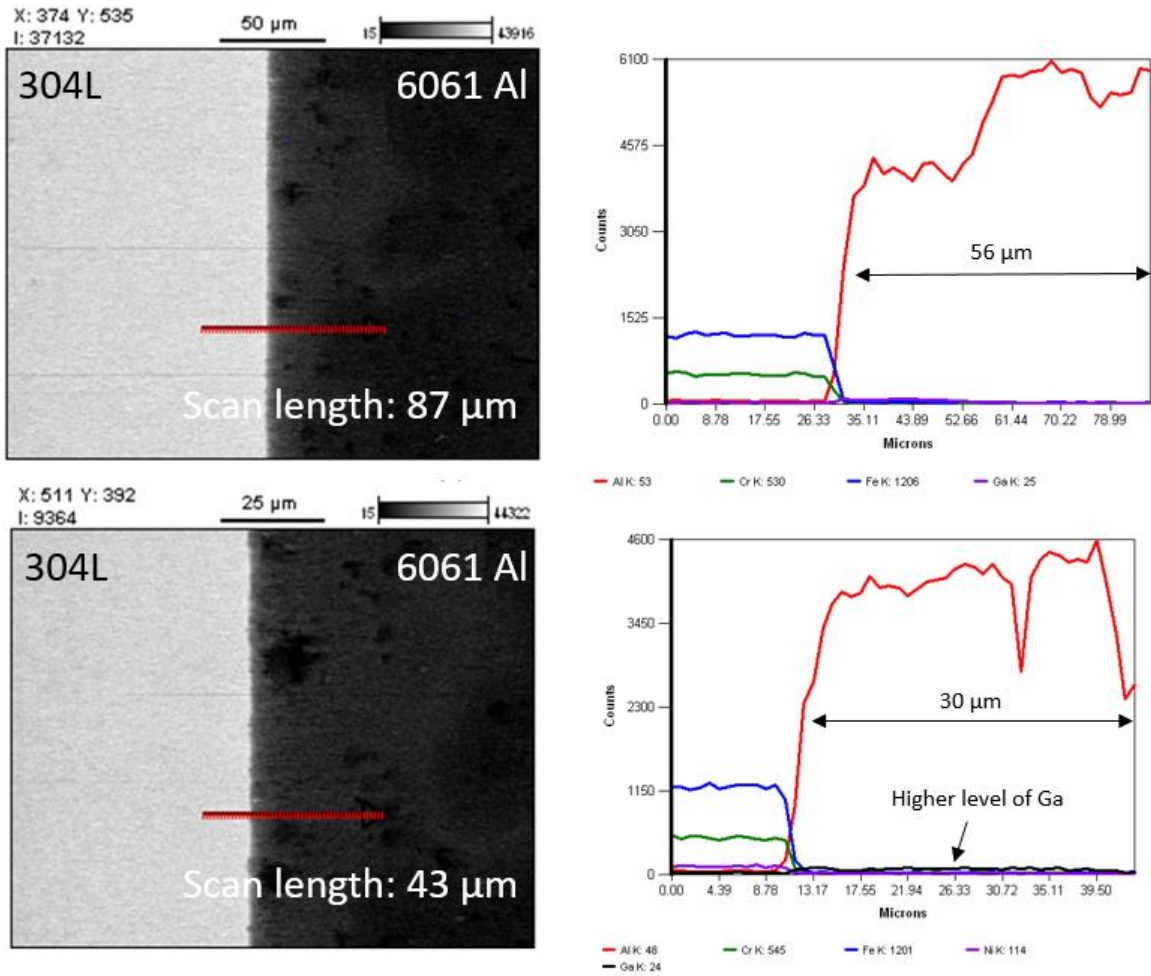
Figure 30. Results for line 1 and line 2 of joint 304L SS/Ga/6061 Al bonded at 330°C for six hours.

Further characterization of the distribution of Ga, Fe, Al, Cr, and Ni around the joint near the bonding region was performed by point analyses at the spots shown in Figure 31. The sample used was the 304L SS/Ga/6061 Al bonded at 330°C for six hours. The detailed concentration of elements is listed in Table VII. Point 3 is composed of 13.58 wt.% Ga, 86.08 wt.% Al; point 4 is composed of 14.47 wt.% Ga, 84.82 wt.% Al; and point 5 is composed of 14.47 wt.% Ga, 84.82

wt.% Al. Further, 1.28 wt.% Ga on point 7 and 1.57 wt.% Ga on point 6 were observed. The high values of Ga concentration on points 3, 4, and 5 confirm that a Ga-rich reaction layer formed on the 6061 Al side; and the results from point 6 and 7 reveals the widely diffusion of Ga on 6061 Al side. On the 304L side, however, only 0.33 wt.% Ga was found on point 1, and no Ga was identified on point 2, indicating a much smaller diffusion of Ga. The chemical compositions of the two points are very close to the composition of 304L stainless steel. This also indicates a limited diffusion of Al on the 304L side. The significant difference in diffusion between Al in 1020 steel and Al in 304L may result from the different crystal structures of 1020 steel and 304L SS steel; the 304L is face-centered cubic (close pack) whereas 1020 steel has a body-centered cubic crystal structure. Thus Ga and Al may diffuse much more easily in BCC 1020 steel than in close-packed 304L steel.
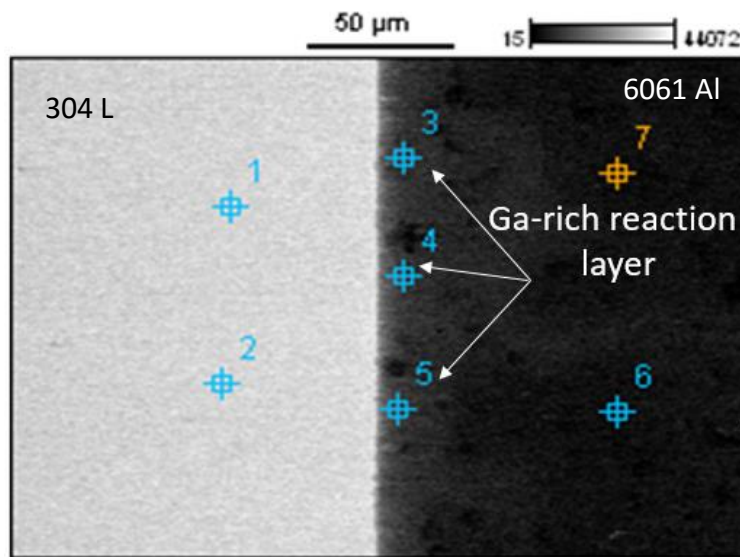
Figure 31. Chemical composition analysis of joint 304L SS/Ga/6061 Al bonded at 330 ºC for six hours.

TABLE VII
CONCENTRATION OF ELEMENTS

330 C-6hour	Weight %				
spectrum point	Al	Cr	Fe	Ni	Ga
1	0.21	18.68	72.62	8.16	0.33
2	0.17	19.11	73.17	7.55	0
3	86.08	0.16	0.18	0	13.58
4	84.82	0.18	0.39	0.14	14.47
5	85.23	0.07	0.48	0	14.22
6	98.55	0	0.12	0.05	1.28
7	97.94	0.15	0.28	0.06	1.57

Figure 32 shows the distribution of alloy elements. The detailed concentration of elements are listed in Table VIII. Results were generated from the EDS spectrum of 7-point analysis across the bonding interface of joint 304L/Ga/6061 Al bonded at 330 ℃ for six hours. It can be seen that Ga is widely diffused in the 6061 Al base, whereas limited diffusion of alloys occurred at a narrow centerline region, also confirming that the interface consists of a narrow reaction layer (around 5μm) on the 304L side and a wider Ga-rich reaction layer (around 60 5μm) on the 6061 Al side.
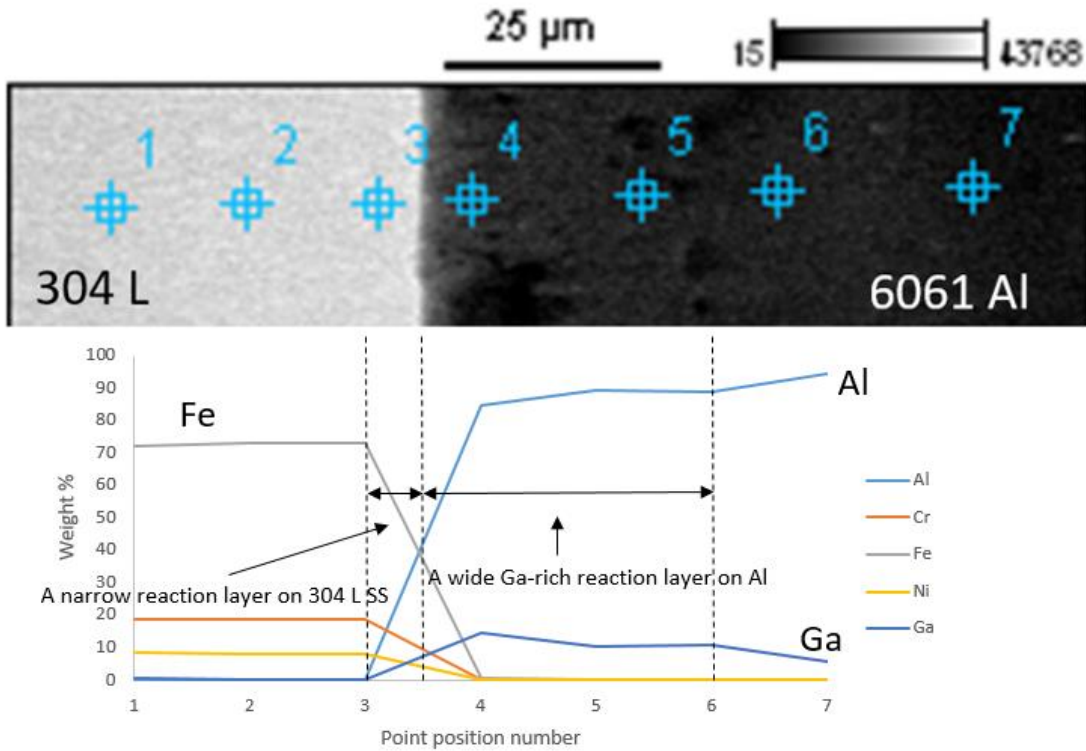
Figure 32. Distribution of alloy elements of joint 304L SS/Ga/6061 Al bonded at 330°C for six hours.

TABLE VIII.
CONCENTRATION OF ELEMENTS.

330 C for 6 hours	Weight %				
Spectrum	Al	Cr	Fe	Ni	Ga
1	0.18	18.76	72.29	8.33	0.44
2	0.05	18.6	73.27	8.05	0.02
3	0.18	18.69	73.08	8.05	0
4	84.72	0.2	0.58	0.03	14.46
5	89.41	0.06	0.12	0.13	10.28
6	88.84	0.15	0.08	0.3	10.63
7	94.28	0.11	0.05	0	5.56

On Al (spectrum 4–7)

X-ray mapping (in Figure 33) shows that the distribution of Ga is wide and far on the 6061 Al side and limited on the 304L side. This widely diffused Ga confirms the wider reaction layer on 6061 Al. X-ray mapping (in Figure 34) of Al, Fe, Cr, and Ni indicates limited diffusion of those elements because less reaction occurred on the 304L SS side.
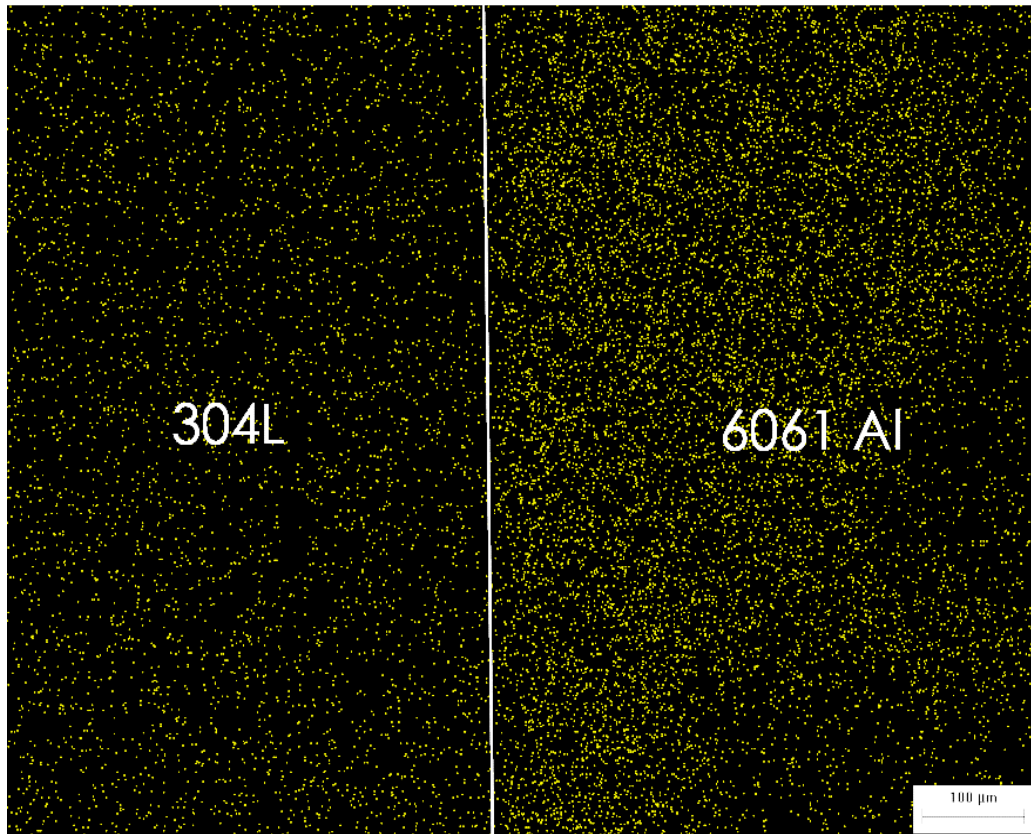
Figure 33. X-ray mapping for Ga of sample 304L SS/Ga/6061 Al bonded at 330°C for six hours.
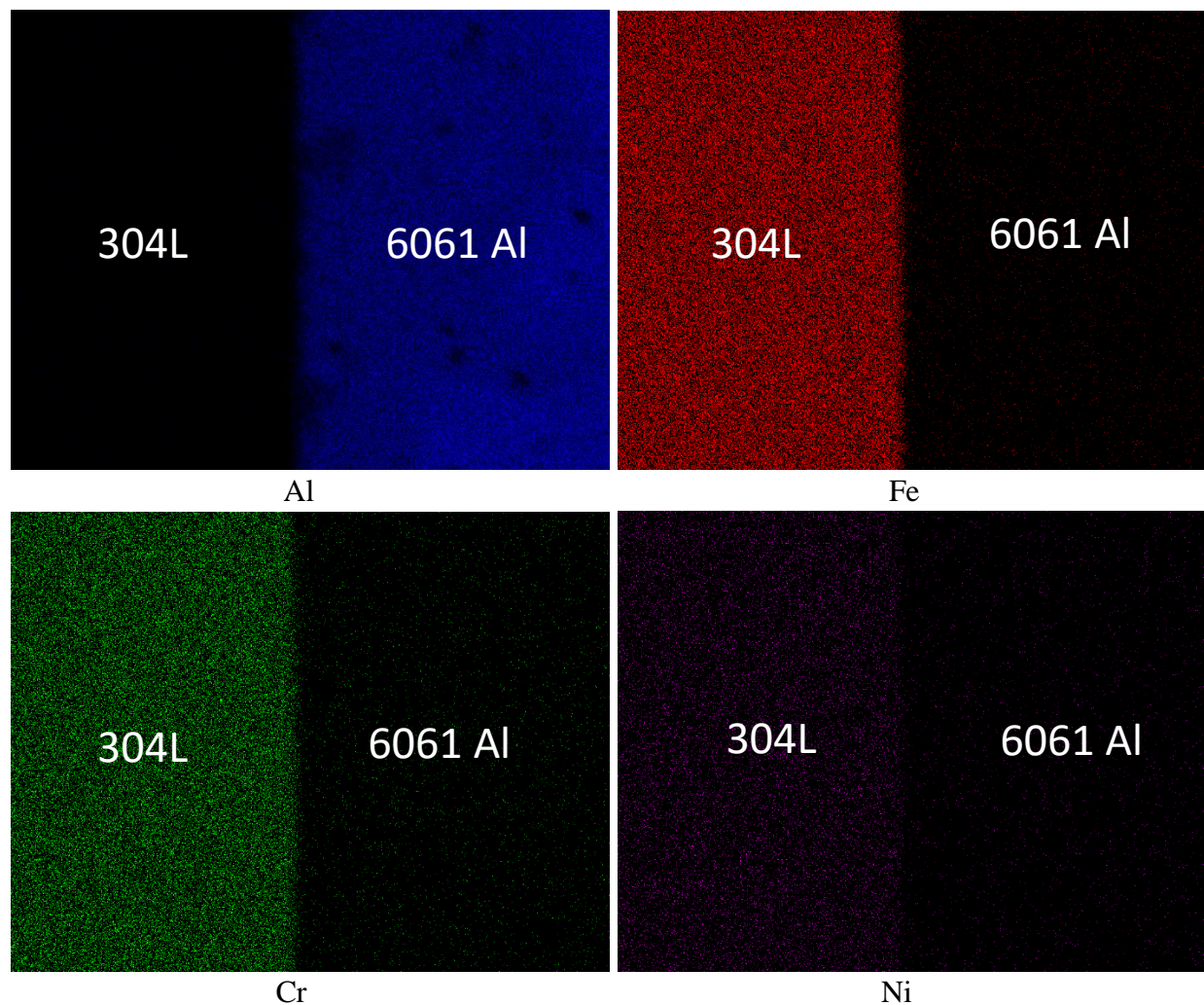
Figure 34. X-ray mapping for Al, Fe, Cr, and Ni of sample 304L SS/Ga/6061 Al bonded at 330°C for six hours.

Diffusion coefficients of Al in 304L, Fe in 6061 Al, and Ga in both base metals (304L and 6061 Al) were roughly estimated based on the data received. The results are shown in Table IX. Diffusion coefficient of Ga in 6061 Al is highest among all the elements investigated, and the high diffusion of Ga into 6061 Al led to the wider reaction layer on the 6061 Al side.

TABLE IX
ESTIMATED DIFFUSION COEFFICIENTS OF THE SAMPLE BONDED AT 330 ^{O}C FOR
SIX HOURS.

304l/Ga/6061 at 330°C for 6 hours	D (m^2/s)
Fe in 6061 Al	5.12E-15
Al in 304l	4.06E-15
Ga in 6061 Al	2.46E-14
Ga in 304l	4.10E-15

4.3   Micro-hardness Testing Results

Micro-hardness testing was conducted on both 1020 steel/Ga/6061 Al samples and 304L
/Ga/6061 Al samples. Indentations were taken from both base metals as well as bonding region.
As shown in Figure 35, distance between each position is 50 μm, and three indentations were made
on every position.
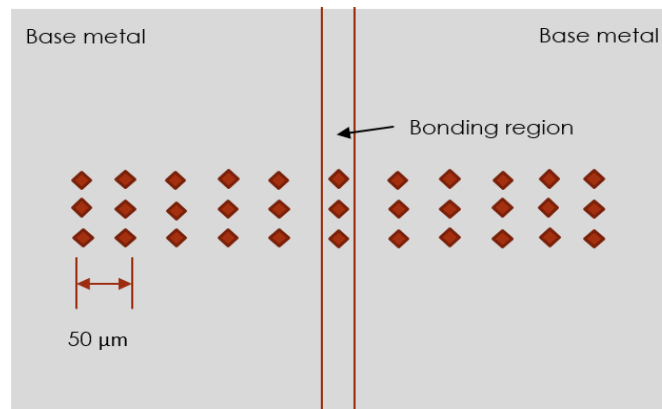
Figure 35. Sketching of indentations.

Averaged hardness results are shown in Figure 36-37. High hardness values were obtained from the bonding region of all 1020 steel/Ga/6061 Al samples. This supports the result discussed earlier that the brittle intermetallic compound Fe_2Al_5 was found in the reaction layers.

For both groups of samples bonded at 480 and 450°C, the averaged hardness on the 6061 Al side is around 85 (Vickers), indicating a slight weakening of the base metal (107 HV for as-received 6061 T6 Al). The averaged hardness on the 6061 Al side where the region was close to the interface (50 μm from centerline) is 71.0 (Vickers). The averaged hardness on the 1020 steel side is 156 (Vickers). As the holding time increases, the reaction layer width increases, and the averaged hardness on the reaction layer increases as well, which indicating the intermetallic formation. All of these combine to produce a more brittle joint. It was shown to be manifested that the cracking found in the bonding regions of the 1020 steel and 6061 Al (Figures 18, 20 and 25). The iron aluminide intermetallics form as the holding time increases.
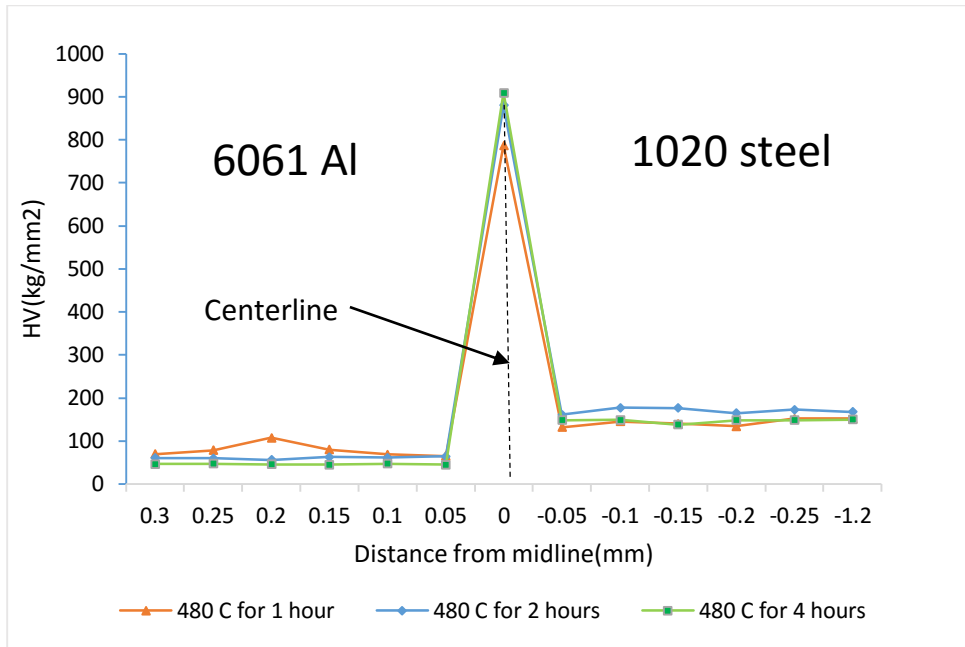
Figure 36. Micro-hardness profile across the joints of 1020 steel/Ga/6061 Al samples bonded at 480ºC.
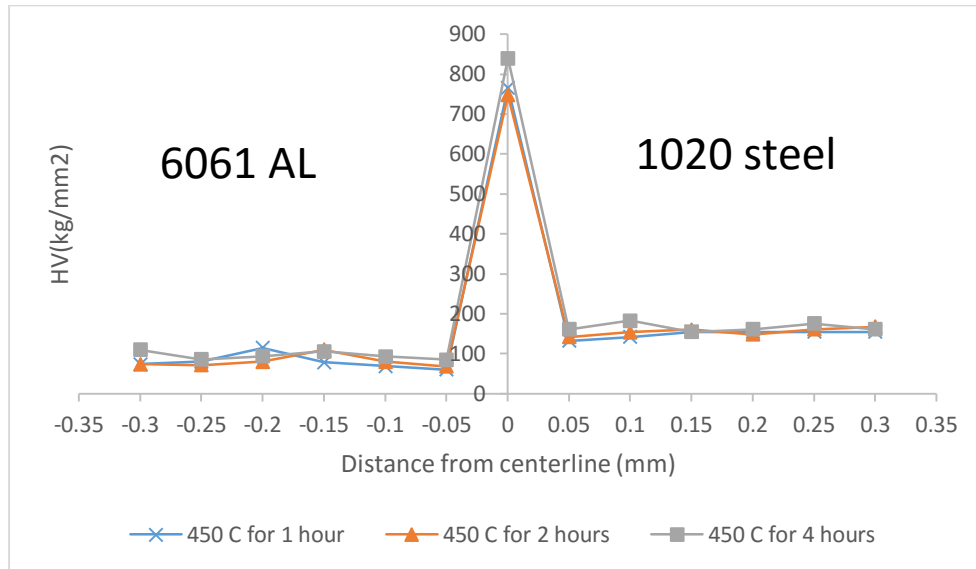
Figure 37. Micro-hardness profile across the joints of 1020 steel/Ga/6061 Al samples bonded at 450ºC.

For the 304L SS/Ga/6061 Al system (shown in Figure 38), no significant peak values were observed on the interlayer, indicating the bonding region is free of IMCs. The hardness of the bonding region drifted because the reaction layers were composed of a narrow layer on the 304L side and a wider layer on the 6061 Al side. Those layers were not uniform; thus, it was hard to access a stable value for those reaction layers.

As shown in Figure 38, all the values on the 6061 Al side were found well below the as-received material that possessed 107 HV. It is possible that the high diffusion of Ga in the Al base metal caused 6061 Al's mechanical properties to weaken. Further, the values of 1020 steel and 304L SS remained similar to the as-received materials, confirming the low diffusion of Ga in those base metals.
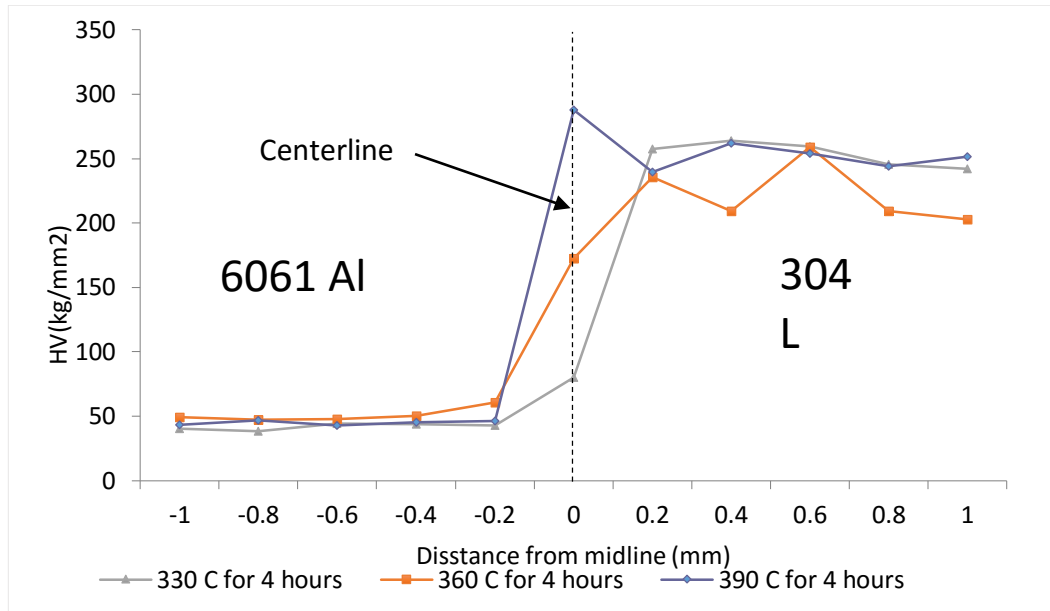
Figure 38. Micro-hardness results of 304L SS/Ga/6061 Al samples.

4.4 Tensile Testing Results.

To determine the optimal parameters for bonding, various processing temperatures and holding times were attempted. Tables X and XI show the joining matrices for the 1020 steel/6061 Al system and the 304L SS/6061 Al system. Bonded specimens were characterized by tensile testing.

For the 1020 steel/6061 Al system (shown in Table X), because of less diffusion, no bonding was achieved at low temperature (400°C), even for a prolonged holding time (six hours). However, because a high bonding temperature (500°C) can result in a thick and brittle interlayer, all joints fractured at the interface with low fracture toughness. A control group (without using Ga) was built for the samples bonded at 450°C; no bonding was achieved at any bonding time.

TABLE X
JOINING MATRIX FOR 1020 STEEL/6061 AL SYSTEM.

1020 /Ga/ Al	Low T	Medium T	High T	1020/No Ga/Al
T (^{o}C)	400	450	500	450
Time (hours)	Up to 6	1, 2, 4	1, 2	1, 2, 4
Highest strength (Mpa)	0	81	33	0
Failure position	no bonding	interface and Al side	interface	No bonding

Similarly, for the 304L SS/Ga/6061 Al system (shown in Table XI), less diffusion, no bonding was achieved at low temperature (270ºC) for a prolonged holding time (12 hours). In contrast, high bonding temperature (450ºC) can lead to overaging of 6061 Al and extensive diffusion of Ga into Al side, causing embrittlement. Although strong bonds were achieved, all the fractures occurred on the Al side at low strength.

TABLE XI
JOINING MATRIX FOR 304L SS STEEL/GA/6061 AL SYSTEM.

304L SS to Al	Low T	Medium T				High T	
T (ºC)	270	300	330	360	390	420	450
Time (hours)	Up to 12	4, 6, 8	4, 6, 8	4, 6, 8	4, 6, 8	1, 2, 3	1, 2, 3
Highest strength (Mpa)	0	62	100.14	51	54	44	49
Failure position	no bonding	interface and Al side				Al side	

4.4.1   Tensile Testing Results of 1020 Steel/Ga/6061 Al System

Among the 1020 steel/Ga/6061 Al system, the sample bonded at 450ºC for one hour (shown in Figure 39) possessed the highest tensile strength. Not only did the specimen have the highest strength, but it also produced the most elongation before its fracture. The fracture image is shown in Figure 40(a): cracking took place on the 6061 Al side and ductile facture was observed, and the fact that the "necking" occurred during loading suggests that 6061 Al's mechanical property was partially reserved. The sound bonding can be attributed to the limited formation of the intermetallic compound layer; however, the weakening on the 6061 Al side was identified.

At this temperature of 450ºC, as the holding time increases, the bonding appears weaker and more brittle. In the case of the sample bonded at 450ºC for two hours, as shown in Figure 40(b), the failure occurred at the interfaces, but distortions were observed on the Al side, indicating

a combination of brittle and ductile fracture mechanism. The weaker bonding is due to the embrittlement of a wider reaction layer. In the case of the sample bonded at 450°C for four hours, as shown in Figure 40(c), the failure also took place at the interfaces, but no distortions were detected in the base metals. The fracture mechanism is completely brittle. Figure 41 shows the fracture path of the sample bonded at 450°C for four hours. The cracking propagated along the interface. In addition, a considerable number of small cracks and elongated voids were found within the interface, which also proved the reaction layer's brittle property. As discussed before, micro-cracks along the joint were first observed on the SEM image (Figure 25) for the sample bonded at 450°C for four hours. Consequently, a thick, brittle interface is the preferred site for crack propagation.

At this temperature (450°C), the best holding time was determined to be one hour, because it limited the formation of brittle intermetallic layer. Prolonged holding time can result in a thicker and brittle reaction layer thereby reducing the joint's mechanical properties.
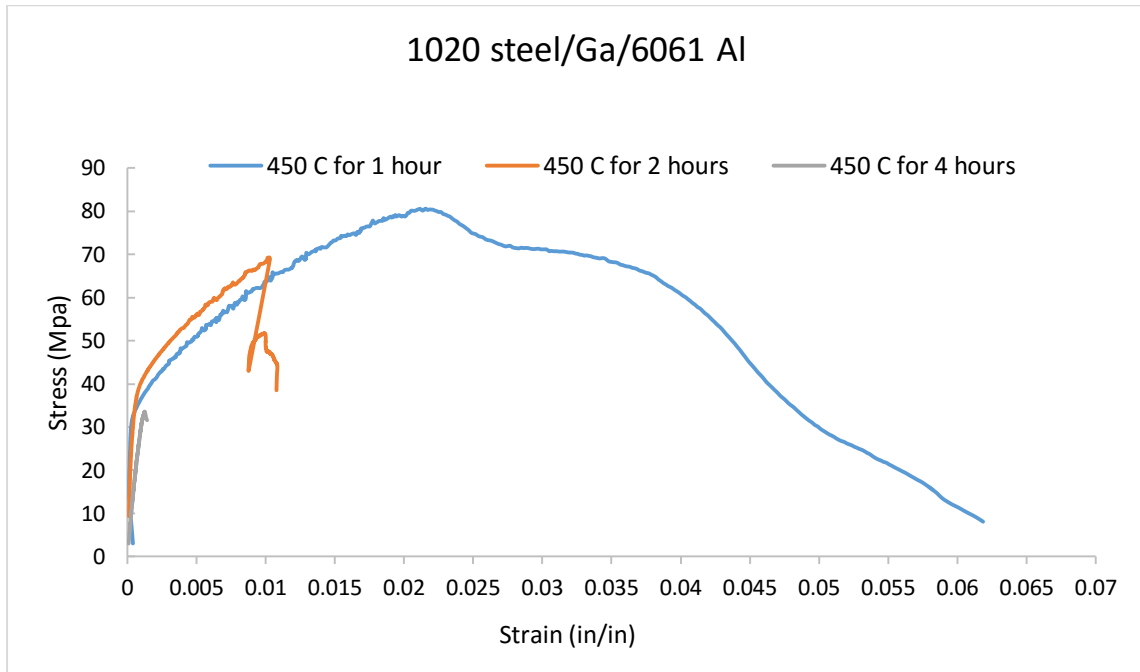
Figure 39. Tensile results of bonded joints of 1020 steel/Ga/6061 Al system.
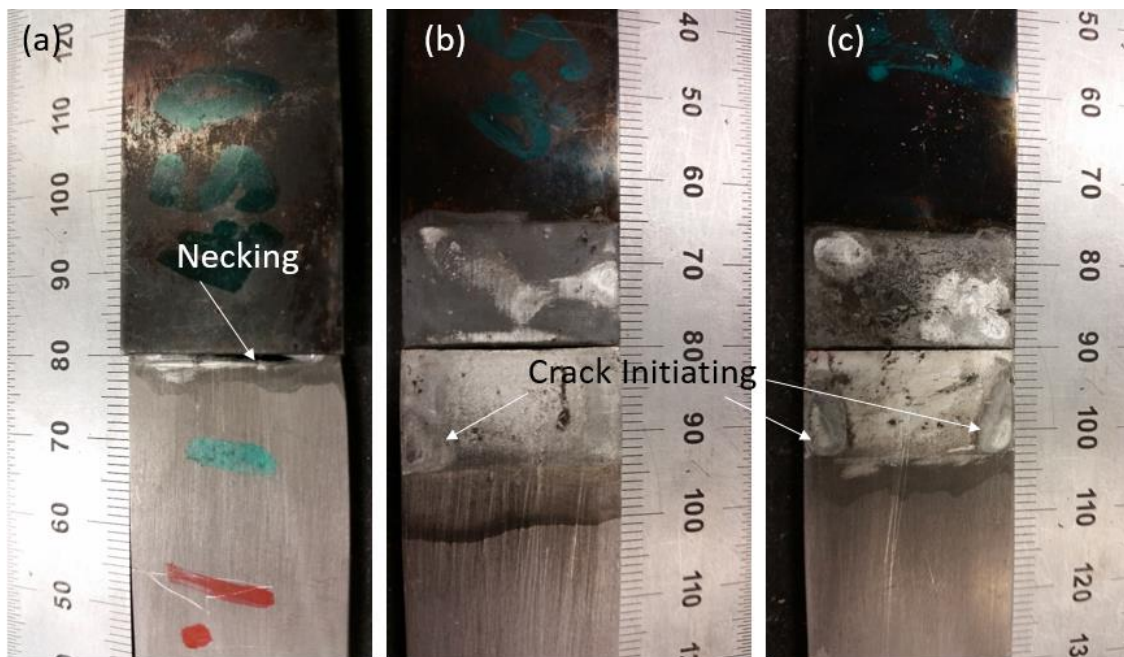
Figure 40. Images of fractures: (a) sample bonded at 450ºC for one hour, (b) sample bonded at 450ºC for two hours, and (c) sample bonded at 450ºC for four hours.
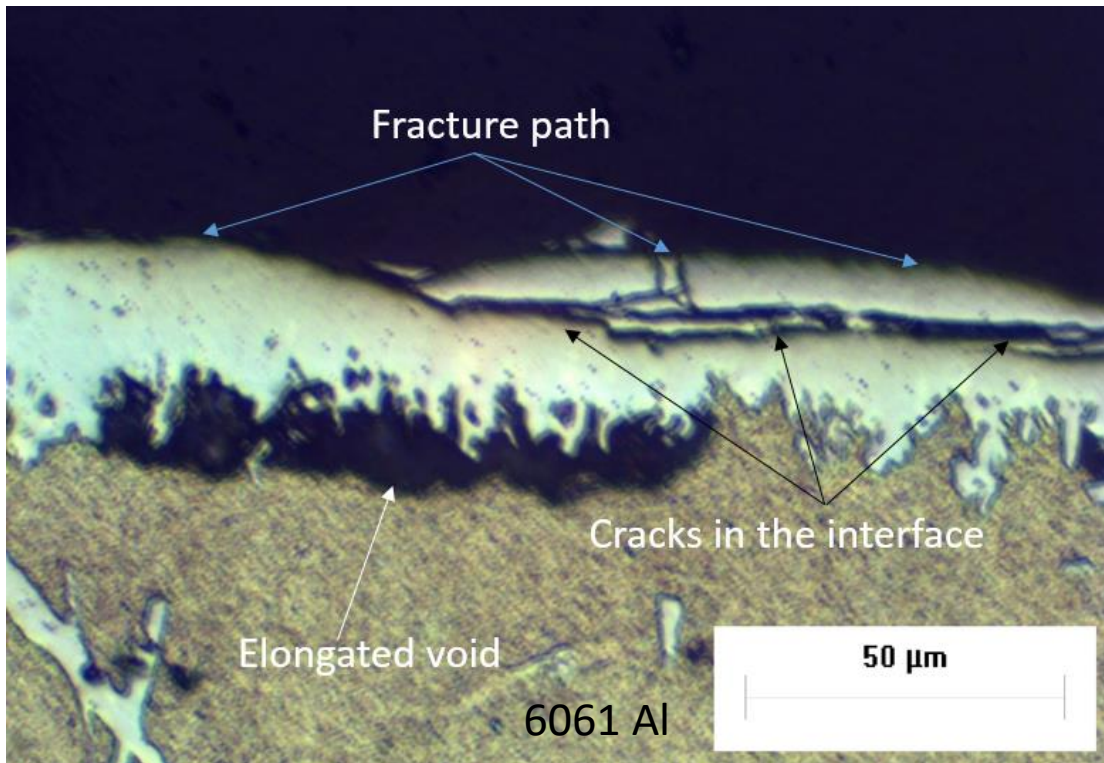
Figure 41. Image of fracture path of joint bonded at 450°C for four hours.

4.4.2 Tensile Testing Results of 304L SS/Ga/6061 Al System

Figure 42 shows tensile data for the 304L SS/Ga/6061 Al system. A Weak bond was obtained for sample bonded at 330°C for 4 hours, the sample fractured at the beginning of loading, no deformation was observed neither on 304L side nor on 6061 Al side, as shown in Figure 43 (a), indicating a brittle fracture from lack of bonding within a short holding time. The fracture path was smooth; as shown in Figure 44, the image confirms a limited reaction layer on the 6061 Al side. The specimen bonded at 330°C for six hours possesses the highest tensile strength. A brittle fracture was observed on the Al side in Figure 43(b); the corresponding curve shown in Figure 37

indicates weakening of both strength and ductility (1.4%) on Al. The sample bonded at 330°C for eight hours possesses the highest ductility (3%); however, as shown in Figure 43 (c), the crack started on the 6061 Al, then propagated into the bonding region, and finally caused the whole bonding to fracture. The tensile strength was measured as 58.3 MPa, indicating a worse weakening on the Al side.
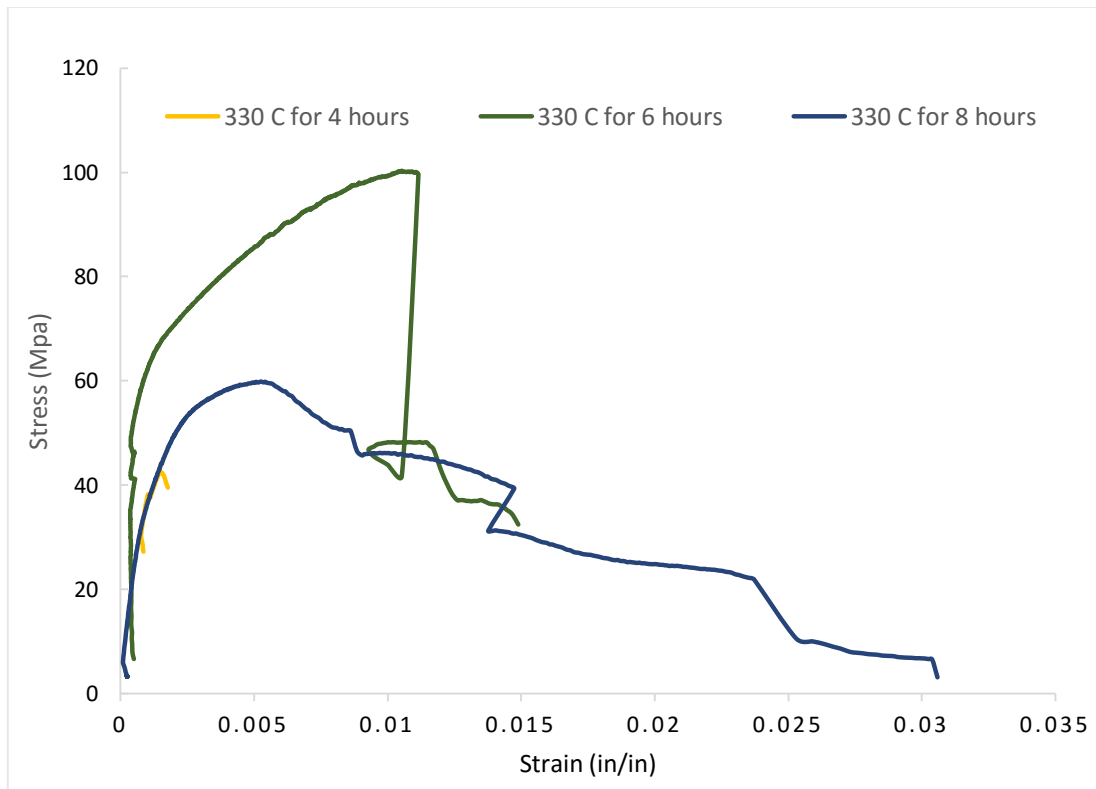
Figure 42. Tensile results of 304L SS/Ga/6061 Al system.
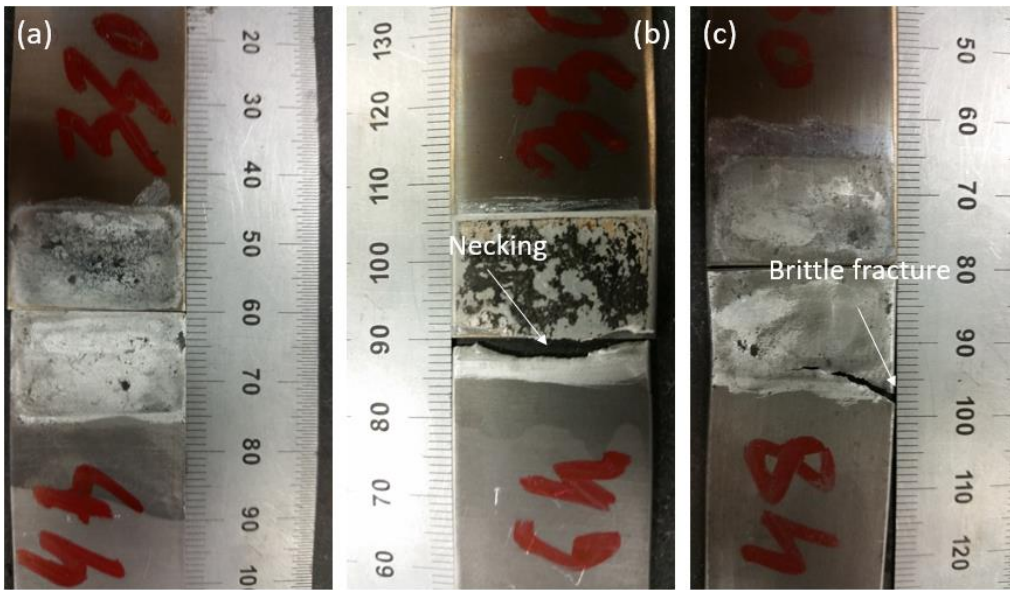
Figure 43. Images of fractures: (a) sample bonded at 330°C for four hours, (b) sample bonded at 330°C for six hours, and (c) sample bonded at 330°C for eight hours.
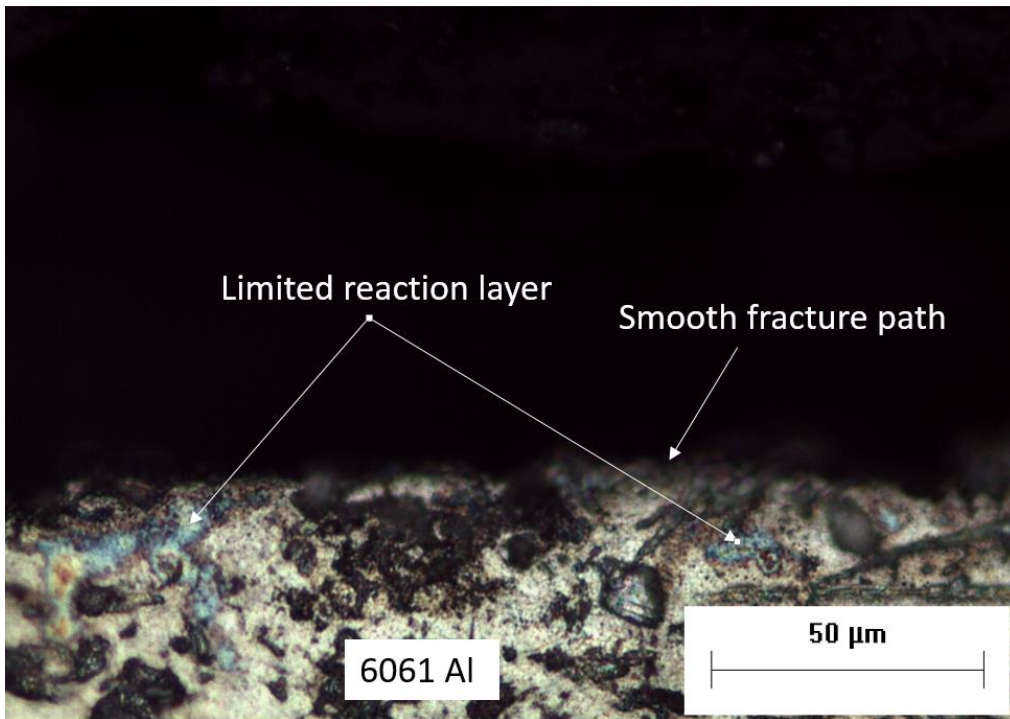

Figure 44. Fracture path of 304L SS/Ga/6061 Al joint bonded at 330°C for four hours.

Thus, in the case of 304L SS/Ga/6061 Al system, a moderate holding time at this temperature (330°C) is preferable. A short holding time will limit alloy diffusion, resulting in inadequate bonding, whereas a prolonged holding time will cause an intensive diffusion of Ga into 6061 Al and strongly weaken the 6061 Al base metal.

For the 1020 steel/Ga/6061 Al system, a sample bonded at 450°C for one hour achieved the best tensile strength. The sample possessed 80.62 MPa of tensile strength and 6.1% elongation at breaking. For the 304L SS/Ga/6061 Al system, a sample bonded at 330°C for four hours achieved the best tensile strength. The sample possessed 100.14 MPa of tensile strength and 1.4% elongation at breaking.

The two samples both fractured on the 6061 Al side. The best tensile results and corresponding strain were shown in Figure 45 and Figure 46. When the results of the two bonding systems were compared with as-received 6061 Al, a weakening and embrittlement of bonded 6061 Al were noticed.
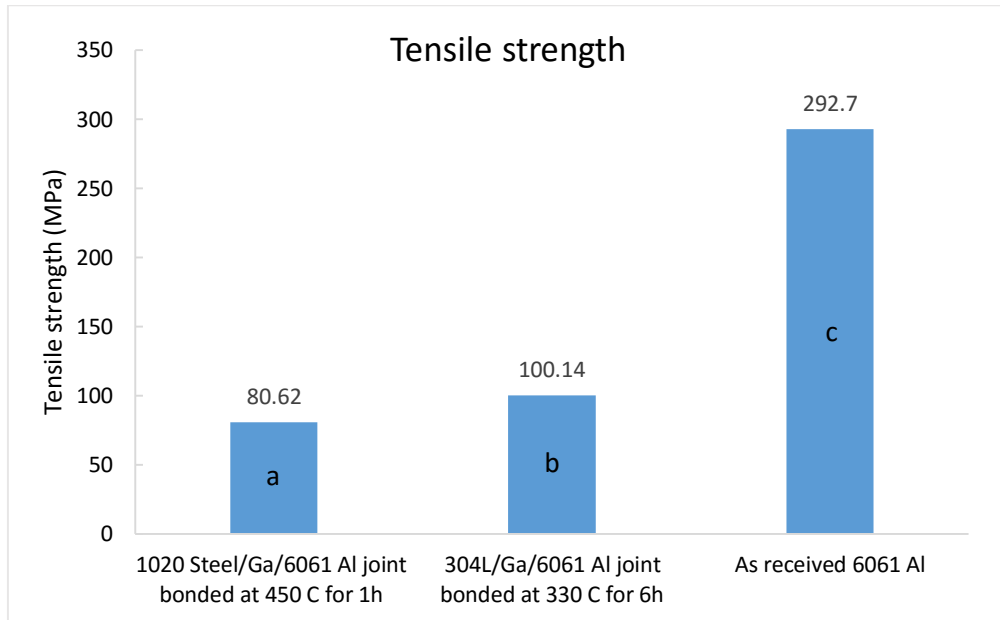
Figure 45. A comparison of the highest tensile results of bonding systems and as-received 6061 Al: (a) 1020 steel/Ga/6061 Al sample bonded at 450°C for one hour, (b) 304L SS/Ga/6061 Al sample bonded 330°C for six hours, and (c) as-received 6061 Al.
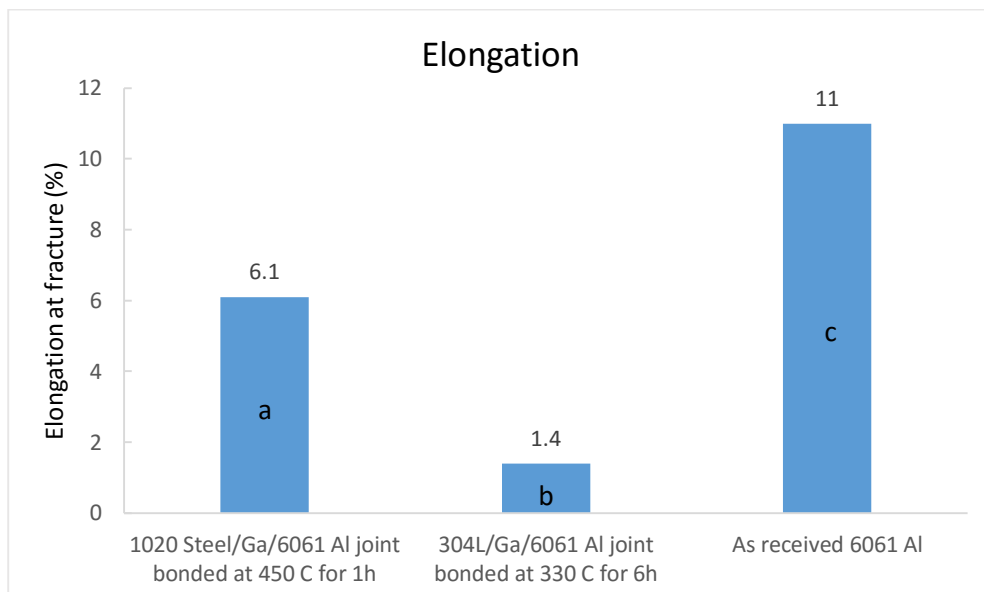
Figure 46. Elongation of bonding systems and as-received 6061 Al: (a) 1020 steel/Ga/6061 Al sample bonded at 450°C for one hour, (b) 304L SS/Ga/6061 Al sample bonded 330°C for six hours, and (c) as-received 6061 Al.

4.5   Effect of Overaging on 6061-T6 Al

Fractures on the 6061 Al side of joints were detected during the tensile testing. The as received 6061-T6 Al alloy is precipitation hardened under full-aged condition. Thus, to understand how heating caused the weakening, the effect of overageing during the bonding process was investigated. Tensile testing was performed on 6061 Al samples heated at 330°C for one, six, and 30 hours. Tensile strength and elongation at the fracture of 6061 Al held at a temperature of 330°C are shown in Figures 47 and 48. As the heating time increased, the tensile strength decreased and the elongation increased. The loss of strengthening and the increase of elongation indicated the overaging of 6061 Al.
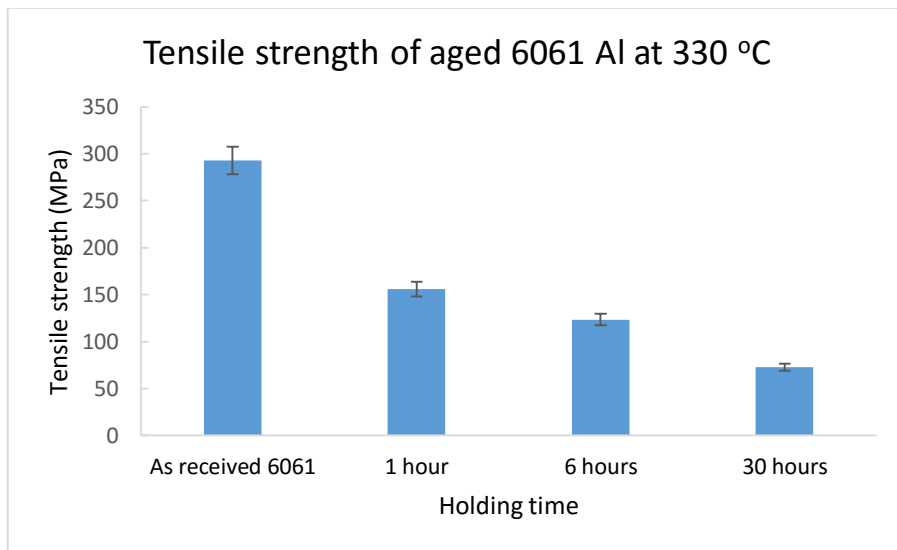
Figure 47. Tensile strength of aged 6061 Al at 330°C and as received 6061 Al.
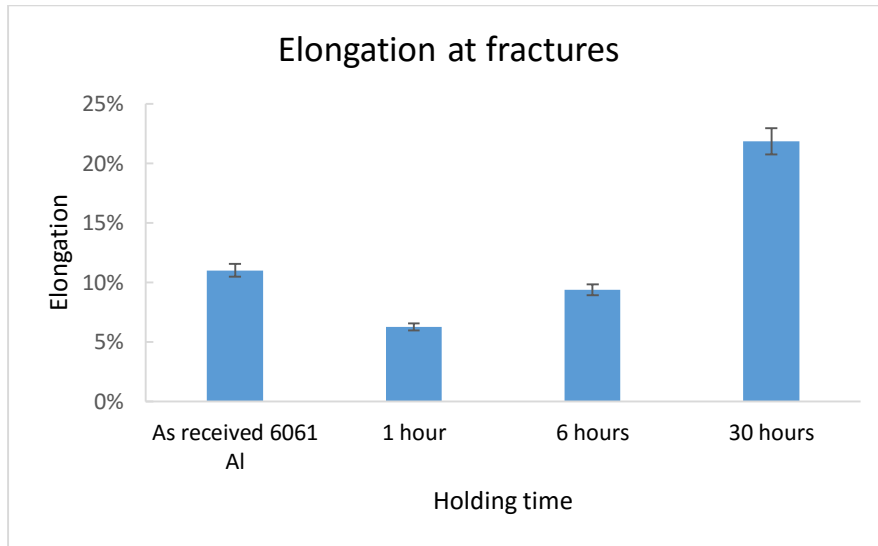
Figure 48. Elongations of aged 6061 Al at 330ºC and as received 6061 Al.

Consequently, in this work, to minimize the effect of overaging, a low bonding temperature and a short bonding time are favorable. However, the optimal combination of processing temperature and holding time must be carefully determined because low temperature and short holding time will lead to inadequate diffusion, whereas high temperature and long holding time can result in unfavorable reactions and overaging of Al.

5. CONCLUSIONS

1. Sound joints were obtained for both 1020 steel/Ga/6061 Al systems and 304L SS/Ga/6061 Al systems. The highest tensile strength of 80.0 MPa was measured for 1020 steel/Ga/6061 Al joints when processed at 450°C for one hour. The highest tensile strength of 100.0 MPa was measured for 304L/Ga/6061 Al joints bonded at 330°C for four hours.

2. In 1020 steel/Ga/6061 Al-T6 TPL joints, Ga was found to promote the diffusion of Al and Fe. The data of joint (bonded at 450°C for 4 hours) show that the diffusion coefficient of both Al in Fe and Fe in Al with Ga are three orders of magnitude higher than the ones without Ga.

3. Hard intermetallic compounds were formed on the reaction layers of 1020 steel/Ga/6061 Al samples. No brittle IMC was identified on 304L SS/Ga/6061 Al samples.

4. The weakening of mechanical properties on 6061 Al observed from both systems is due to overaging and the embrittlement caused by the excessive amount of Ga that segregated into the Al.

REFERENCES

1. Elaheh Ghassemieh, Marcello Chiaberge, Materials in automotive application, state of the art and prospects. New Trends and Developments in Automotive Industry. Rijeka, In Tech, 2011, pp. 365-367.

2. P. E. George. (2009, Oct. 5th), Top 5 materials used in auto manufacturing. [Online]. Available: http://howstuffworks.com.

3. M.L. Kuntz, Y. Zhou, and S.F. Corbin, A study of transient liquid-phase bonding of Ag-Cu using differential scanning calorimetry. Metallurgical and materials transactions. Vol. 37, 8 (2006), pp. 2493-2504.

4. G. Kobe, Aluminum/steel welding, Automotive Industries, Vol. 7 (1994), p. 44.

5. Tatsuya Sakiyama, Dissimilar Metal Joining Technologies for Steel Sheet and Aluminum Alloy Sheet in Auto Body, Nippon Steel Technical Report, No. 103, May 2013.

6. J. Ma, M. Harooni, B. Carlson, R. Kovacevic, Dissimilar joining of galvanized high-strength steel to aluminum alloy in a zero-gap lap joint configuration by two-pass laser welding, Mater Des, Vol. 58 (2014), pp. 390-401.

7. M. Hansen, K. Anderko, H.W. Salzberg, Constitution of binary alloys, McGraw-Hill Book Company, New York (1958).

8. M.J. Rathod, M. Kutsuna, Joining of aluminum alloy 5052 and low-carbon steel by laser roll welding, Welding Journal, Vol. 83 (2004), pp. 16-S.

9. A. Mathieu, S. Pontevicci, J.C. Viala, E. Cicala, S. Matteï, D. Grevey, Laser brazing of a steel/aluminium assembly with hot filler wire (88% Al, 12% Si), Mater Sci Eng A, Vol. 435 (2006), pp. 19-28.

10. S. Frank, Flux-free laser joining of aluminum and galvanized steel, Journal of Materials Processing Technology, Vol. 222 (August 2015), pp. 365-372.

11. A. Mathieu, S. Mattei, A. Deschamps, B. Martin, D. Grevey, Temperature control in laser brazing of a steel/aluminium assembly using thermographic measurements, NDT&E Int., Vol. 39 (2006), pp. 272-276.

12. T.J. Lienert, J.R.W.L. Stellwag, B.B. Grimmett, R.W. Warke Friction stir welding studies on mild steels Welding Journal Supplement, Vol. 82 (2003), pp. 1S-9S.

13. A.P. Reynolds, W. Tang, T. Gnaupel-Herold, H. Prask Sturcture, properties, and residual stress of 304L stainless steel friction stir welds Scripta Materialia, Vol. 48 (2003), pp. 1289-1294.

14. Wei Liu, Junjie Ma, Joining of advanced high-strength steel to AA 6061 alloy by using Fe/Al structural transition joint, Materials & Design, Vol. 68, 5 (March 2015), Pages 146-157.

15. R. D. Jadeja, T. M. Shaikh, A review on experimental and numerical investigation of friction stir welds of AA6063-T6 aluminum alloy, International Journal of Advanced Engineering Research and Studies, Vol. 2 (2012), pp. 123-127.

16. M.J. Rathod, M. Kutsuna, Joining of aluminum alloy 5052 and low-carbon steel by laser roll welding, Welding Journal, Vol. 83 (2004), pp. 16-26.

17. S. Katayama, Laser welding of aluminum alloys and dissimilar metals, Welding International, Vol. 18 (2004), pp. 618-625.

18. O. Kubaschewski, Iron-binary phase diagrams. Springer-Verlag Berlin, Aachen, 1982, p. 5.

19. Grant O. Cook III • Carl D. Sorensen, Overview of transient liquid phase and partial transient liquid phase bonding, Journal of materials science. Vol. 46 (2011), pp. 5305-5323.

20. Tuah-Poku, Massalski, and T. B. Massalski, A study of the transient liquid phase process applied to an Ag/Cu/Ag sandwich joint, Metall. Trans. Vol. 19, A(3) (1988), pp. 675-686.

21. W. D. MacDonald and T. W. Eagar, Transient liquid phase bonding, Annual Review of Materials science, Vol. 22 (1992), pp. 23-46.

22. Hidetaka Umeshita, Effects of alloying elements on interfacial properties of dissimilar joint of aluminum alloy and steels, Smart processing technology, Vol. 2 (2008), pp. 199-202.

23. Masaki Koba, Toshio Araki, Bonding interface formation between Mg alloy and steel by liquid-phase bonding using the Ag interlayer, Metals & Materials Society and ASM International. Vol. 43 (2012), pp. 592-597.

24. Wu Ming-fang, Si Nai-chao, Contact reactive brazing of Al alloy/Cu/stainless steel joints and dissolution behaviors of interlayer, Trans. Nonferrous Met. Soc. China, Vol. 21 (2011), pp. 1035-1039.

25. E. Lee, O. Quintana, J. E. Indacochea, Joining of aluminum sheets by combined solid state and TLP bonding processes, Science and technology of welding and joining, Vol. 18 (2013), pp. 98-102.

26. Jun-Yen Uan and Cheng-Chia Chang, Gallium-induced magnesium enrichment on grain boundary and the gallium effect on degradation of tensile properties of aluminum alloys, Metallurgical and materials transactions, Vol. 37 (2006), pp. 2133-2145.

27. Michael Bauccio, ASM Metals Reference Book. ASM International, Materials Park, OH, 1993.

28. H. Okamoto, The Fe-Ga system, Bulletin of Alloy Phase Diagrams, Vol. 11, 6 (1990), p. 577.

29. J. L. Murray, The Al-Ga system, Bulletin of Alloy Phase Diagrams, Vol. 4, 2 1983, p. 184.

30. Howard E. Boyer and Timothy L. Gall, Metals Handbook, American Society for Metals, Materials Park, OH, 1985.

31. R.R. Ambriz and D. Jaramillo, Mechanical Behavior of Precipitation Hardened Aluminum Alloys Welds, Light Metal Alloys Applications. Rijeka, InTech, 2014, pp. 35-57.

32. Katharine B. Small, David A. Englehart, and Todd A. Christman, Guide to Etching Specialty Alloys, Advanced Materials & Processes, Vol. 166, 2 (2008), pp. 32-37.

33. William D. Callister, Jr. and David G. Rethwisch, Materials Science and Engineering an Introduction (8th edition), Hoboken, Donald Fowley, pp. 128-129.

VITA

NAME:	Yuke Wang
EDUCATION:	B.S., Materials Engineering, Chongqing University of Technology, Chongqing, China, 2011. M.S., Materials Engineering, University of Illinois at Chicago, Chicago, Illinois, 2015.
EXPERIENCE	Department of Civil and Materials Engineering, University of Illinois at Chicago: Teaching assistant, 2013-2015.
HONORS:	Chongqing University of Technology: Second prize of Students' Academic Science and Technology Paper Competition 2011.
PROFESSIONAL MEMBERSHIP:	American Society of Materials.